Biomaterials 192 (2019) 245–259

Contents lists available at ScienceDirect

Biomaterials

journal homepage: www.elsevier.com/locate/biomaterials

Dual carrier-cargo hydrophobization and charge ratio optimization improve the systemic circulation and safety of zwitterionic nano-polyplexes

Meredith A. Jackson[a], Sean K. Bedingfield[a], Fang Yu[a], Mitchell E. Stokan[a], Rachel E. Miles[a], Elizabeth J. Curvino[a], Ella N. Hoogenboezem[a], Rachel H. Bonami[b], Shrusti S. Patel[a], Peggy L. Kendall[c], Todd D. Giorgio[a], Craig L. Duvall[a,*]

[a] Department of Biomedical Engineering, Vanderbilt University, Nashville, TN, USA
[b] Department of Medicine, Division of Rheumatology and Immunology, Vanderbilt University Medical Center, Nashville, TN, USA
[c] Department of Medicine, Division of Allergy, Pulmonary, and Critical Care, Vanderbilt University Medical Center, Nashville, TN, USA

ARTICLE INFO

Keywords:
RNA interference
Zwitterionic polyplexes
Dual hydrophobization
Pharmacokinetics
Toxicology
Drug delivery

ABSTRACT

While polymeric nano-formulations for RNAi therapeutics hold great promise for molecularly-targeted, personalized medicine, they possess significant systemic delivery challenges including rapid clearance from circulation and the potential for carrier-associated toxicity due to cationic polymer or lipid components. Herein, we evaluated the *in vivo* pharmacokinetic and safety impact of often-overlooked formulation parameters, including the ratio of carrier polymer to cargo siRNA and hydrophobic siRNA modification in combination with hydrophobic polymer components (dual hydrophobization). For these studies, we used nano-polyplexes (NPs) with well-shielded, zwitterionic coronas, resulting in various NP formulations of equivalent hydrodynamic size and neutral surface charge regardless of charge ratio. Doubling nano-polyplex charge ratio from 10 to 20 increased circulation half-life five-fold and pharmacokinetic area under the curve four-fold, but was also associated with increased liver enzymes, a marker of hepatic damage. Dual hydrophobization achieved by formulating NPs with palmitic acid-modified siRNA (siPA-NPs) both reduced the amount of carrier polymer required to achieve optimal pharmacokinetic profiles and abrogated liver toxicities. We also show that optimized zwitterionic siPA-NPs are well-tolerated upon long-term, repeated administration in mice and exhibit greater than two-fold increased uptake in orthotopic MDA-MB-231 xenografts compared to commercial transfection reagent, *in vivo*-jetPEI®. These data suggest that charge ratio optimization has important *in vivo* implications and that dual hydrophobization strategies can be used to maximize both NP circulation time and safety.

1. Introduction

In the last twenty years, RNA-based therapeutics have proceeded from discovery, through extensive development, and to the exciting, recent FDA approval of the first siRNA nanomedicine [1]. This progression has been significantly driven by lipid and polymer-based delivery vehicles. However, when administered intravenously, nucleic acids continue to face well-documented barriers including nuclease degradation, poor cell and tissue uptake, and rapid clearance from circulation, especially in the liver and kidney [2,3]. As a testament to these hurdles, many of the advanced RNA-based therapeutics currently in clinical trials focus on local, carrier-free application or systemic delivery of siRNAs directly conjugated to ligands that drive rapid uptake by hepatocytes in the liver [4].

There is a significant application space for systemically delivered siRNAs against non-hepatic targets. Oncology is a particularly promising field of application for RNAi therapeutics because they can be designed against tumor drivers that are undruggable by conventional small molecule approaches [5–8]. However, there is still a significant gap in the technology needed to make this clinically feasible. Because tumors and target tissues other than the liver receive only a small amount of the total cardiac output, longer nanocarrier circulation times are needed to achieve sufficient biodistribution [9,10]. In fact, there is a close connection between vascular circulation time and level of tumor delivery of nanomedicines [11–17]. Nonviral polymeric siRNA carriers are often employed to improve cell uptake and provide endosomal escape properties, but these carriers are still prone to instability in circulation from serum proteins or, in the case of electrostatically-assembled formulations, anionic heparan sulfates which are highly concentrated in the kidney, reducing the opportunity for carriers to

* Corresponding author.
E-mail address: craig.duvall@vanderbilt.edu (C.L. Duvall).

https://doi.org/10.1016/j.biomaterials.2018.11.010
Received 21 September 2018; Received in revised form 8 November 2018; Accepted 9 November 2018
Available online 10 November 2018
0142-9612/

distribute intact to target sites such as tumors [18–20].

Polymeric and lipid carriers often incorporate hydrophilic surface coatings, such as PEG, that shield the electrostatically-packaged/entrapped siRNA cargo in the nano-formulation interior, but such improvements often only marginally improve circulation stability [21–23]. One of the first clincally tested polymeric siRNA carriers, CALAA-01, was shown to be primarily disassembled in the kidney and cleared completely from circulation by 30 min after intravenous injection in human patients [24]. It also exhibited signs of liver and kidney toxicity in non-human primates and hypersensitivity immune reactions in human patients that were associated primarily with the polymer components (not siRNA) of the formulation [24]. These experiences point to current major limitations in the field of systemic, polymer-based siRNA delivery—limited circulation stability and the potential for carrier-associated toxicity.

In addition to insufficient circulation stability, siRNA nano-formulations are often plagued by dose-limiting toxicities caused by cationic lipids/polymers that can damage cellular membranes or cause aggregation of serum or cellular blood components [21,25]. The design of polymer carriers is often a balancing act between increased silencing efficiency and increased cytotoxicity [26,27]. These toxicities are dose-dependent, and many have sought to ameliorate them through iterative modification of the polymer structure of nanocarriers [28]. The desire to increase the therapeutic window, or the gap between maximum tolerated dose and minimum efficacious dose, has led to a multitude of library-based studies that have examined the relationship between polymer structure and nanocarrier performance [29–31].

With the substantial focus on iterating on polymer structure, the *in vivo* pharmacokinetic and toxicity impact of two important aspects of formulating siRNA nanocarriers are often overlooked—the carrier to cargo ratio ("charge ratio" or "N:P ratio") and stabilizing modifications to siRNA cargo. Few studies have characterized impact of N:P ratio (the ratio of cationic polymer amines to siRNA phosphates) on *in vivo* polyplex pharmacokinetics and toxicity, and those that have are limited exclusively to cationic-only carriers such as polyethylenimine (PEI) and homopolymers of poly(2-(dimethylamino)ethyl methacrylate) (pDMAEMA) [32–34]. In these studies, increasing N:P ratios are accompanied by increases in particle zeta potential, which can increase carrier toxicity by inducing aggregation of blood components and shifting biodistribution from the lungs to liver [33,35]. *In vitro,* increasing N:P ratios can increase both polyplex transfection efficiency and toxicity due to the presence of excess, uncomplexed polymer, but these effects are likely less relevant after systemic administration [36–38]. Little is known about the impact of N:P ratio on *in vivo* circulation half-life and toxicity properties of well-shielded, hydrophobically stabilized polyplexes.

The present study was designed to elucidate the effect of N:P ratio on *in vivo* pharmacokinetics and toxicity profile of siRNA carriers with dual hydrophobic stabilization on both the cationic, siRNA-condensing polymer block and the siRNA cargo. A previously-optimized siRNA-condensing random copolymer block was utilized with balanced (50 mol% of each) hydrophobic (butyl methacrylate (BMA)) and cationic (DMAEMA) monomer content, referred to as "50B"; this polymer provides pH-responsive, endosomolytic properties along with improved circulation stability and *in vivo* bioactivity relative to traditional nanopolyplexes (NPs) made solely from cationic monomers such as P(DMAEMA) [39]. The P(DMAEMA-*co*-BMA) segment was blocked with a super-hydrophilic, zwitterionic phosphorylcholine-based polymer (P(2-methacryloyloxyethyl phosphorylcholine) (P(MPC)) to form the NP corona; we recently showed this composition to achieve superior tumor cell delivery *in vivo* relative to traditional PEG NP surface chemistry [11]. Leveraging this optimized polymer structure containing a balance of cationic and hydrophobic content in the siRNA-condensing block, we explored the effect of varying the polymer:siRNA (N:P) ratio, with and without hydrophobic modification of the siRNA cargo with palmitic acid (PA, $CH_3(CH_2)_{14}COOH$). Additionally, we studied the long-term toxicologic impacts of repeated administration of candidate formulations. Another contribution from this study is that, despite the growing evidence in favor of zwitterionic polymer NP surface coatings as an alternative to PEG, the toxicology of zwitterionic nanocarrier systems is significantly less studied relative to PEGylated systems [11,31,40,41].

Several groups, including ours, have shown that the introduction of hydrophobic moieties improves the stability of polymer-based siRNA delivery systems [12,13,28,39,42]. These strategies have typically involved either modification of the polymer structures or addition of hydrophobic groups such as cholesterol directly onto the siRNA molecules [42–47]. We previously demonstrated that the use of a "dual hydrophobization" strategy in both the carrier polymers and the cargo siRNA could significantly improve the stability and tumor gene silencing ability of PEGylated polyplexes [13]. Here, we further investigate this strategy utilizing zwitterionic NPs, in the context of various charge ratios, and with a deeper focus on toxicological impacts of the interplay between N:P ratio and siRNA hydrophobization. These studies provide unique insights into dual hydrophobization as a strategy to reduce N:P ratio and even to reduce toxicity for a specific N:P relative to polymer-only hydrophobization.

2. Materials and methods

2.1. Materials

Chemicals and materials for biological assays were purchased from Sigma-Aldrich (St. Louis, MO, USA) or Fisher Scientific (Waltham, MA, USA) unless otherwise noted. All oligonucleotides used in these studies were purchased from Integrated DNA Technologies (Coralville, IA, USA). For all studies involving fluorescently-tagged oligonucleotides, dsDNA of 23 base pairs were used as a model for siRNA. The sequences of all oligonucleotides used in these studies can be found in Supplementary Table 1 and referenced in our previous work [12].

2.2. Polymer synthesis

Polymers were synthesized using Reversible Addition Fragmentation Chain Transfer (RAFT) techniques. The RAFT chain transfer agent, 4-(ethylsulfanylthiocarbonyl)sulfanylpentanoic acid, was synthesized using previously described methods [11]. A macroCTA consisting of a random co-polymer of poly(dimethylaminoethyl methacrylate-co butyl methacrylate) [P(DMAEMA-*co*-BMA)] was synthesized using a 50:50 monomer feed ratio, targeting 210 repeat units (expecting 70% conversion), with the goal of achieving 75–80 repeating units of each monomer. Prior to polymerization, all monomers were removed of inhibitors by passing through two activated basic alumina columns. The reaction was stirred under nitrogen at 65 °C for 24 h at 20 wt% in dioxane, using a CTA:initiator ratio of 10:1 (AIBN as initiator). The final reaction was precipitated in cold pentane 3 times, then dried under vacuum. Molecular weights and degree of polymerization were confirmed by 400 MHz ^{1}H NMR in $CDCl_3$ and gel permeation chromatography with DMF mobile phase (0.1 M LiBr; polymer at 10 mg/mL; Agilent Technologies, CA) with Wyatt miniDAWN TREOS light scattering detectors. The dn/dc values for the molecular weight calculation were determined on a refractometer (Abbemat 300, Anton Paar). A corona block of poly(2-methacryloyloxyethyl phosphorylcholine) [P(MPC)] was then RAFT polymerized from the P(DMAEMA-*co*-BMA) macroCTA by targeting a degree of polymerization of 75 (to achieve a 20 kDa block), making the final polymer (referenced as P(MPC-*bl*-(DMAEMA-*co*-BMA))). The reaction was carried out at 20 wt% under nitrogen in methanol (with condenser) at 65 °C for 24 h, with a 5:1 CTA: Initiator ratio (AIBN initiator). The crude reaction was then dialyzed in methanol for one day, followed by water for one day, and lyophilized. Degree of polymerization was confirmed by ^{1}H NMR.

2.3. Conjugation of palmitic acid (PA) to siRNA

Amine-modified siRNA was dissolved in a 50:50 mixture of isopropanol and nuclease-free water to create a 40 nmol/mL concentration in the final reaction (90% of final volume). NHS-modified PA was dissolved in DMF to create a 4000 nmol/mL concentration in the final reaction (DMF volume was 10% of final reaction volume). The PA was added to the siRNA solution, stirring at room temperature, and diisopropyl ethyl amine (DIPEA) was added at 1 μL per mL of final reaction volume. Further additions of PAin DMF and DIPEA were done at 24 h and 48 h. At 72 h, nuclease-free water was added to dilute the DMF to 10% of the total volume, and the mixture was centrifuged for 10 min at $3000 \times g$ to remove precipitated, excess PA. The supernatant was then dialyzed (12 h, 2 solvent changes) in nuclease free water using 3500 MWCO dialysis tubing. The resulting cloudy mixture was passed through a 0.22 μm filter and then lyophilized. The lyophilized powder was re-dissolved in water and passed through another 0.22 μm filter to further remove residual PA. The mixture was then purified on NAP25 columns, frozen, lyophilized, re-dissolved in nuclease-free water, and quantified on a Nanoquant plate (Tecan, Mannedof, Switzerland).

The conjugate molecular weight was confirmed using LC-MS, and purity was verified using reverse-phase HPLC. For conjugate molecular weight, siRNA conjugates were run in negative ionization mode using LC-MS-ESI (Waters Synapt). Samples were run using a Kinetix 1.7 μm PFP 100 A LC Column under a linear gradient from 95% water (10 mM triethylammonium acetate), 5% methanol (10 mM triethylammonium acetate) to 100% methanol. For additional HPLC confirmation of purity, the conjugate was injected at 5–30 nmol in 200 μL solvent, using water with 100 mM TEAA (triethyl ammonium acetate) and methanol in a linear gradient (95% water, 5% methanol to 100% methanol, back to 95% water/5% methanol) and a Clarity Oligo-RP column (Phenomenex, Torrence, CA). Single-stranded PA conjugates were then annealed to antisense siRNA strands using a C1000 Thermal Cycler (Bio-Rad, Hercules, CA).

2.4. Formulation of siRNA NPs

Buffers used for NP formulation were created using the Sigma Buffer Reference Center Online Resource. To form NPs, P(MPC-*bl*-(DMAEMA-*co*-BMA)) polymers were dissolved in 10 mM citric acid buffer (pH = 4) and then added to various amounts of siRNA for 30 min. The amounts of siRNA or PA-siRNA to add were determined using the N:P ratio (10, 15, or 20), which was calculated using the following equation (50% of DMAEMA monomers are assumed to be protonated at pH 7.4:

$$nmol\ polymer = \frac{(nmol\ nucleic\ acid)(base\ pairs\ nucleic\ acid)(2)(N{:}\ P\ ratio)}{(\text{DMAEMA repeat units})(0.5)}$$

After complexing at pH 4 for 30 min, the pH was raised to 7.4 by adding 10 mM sodium phosphate buffer at pH 8 (5:1 v/v ratio). In all cases, unless otherwise noted, polymer was dissolved at an initial concentration of 3 mg/mL. NP formulations with normal siRNA (si-NPs) at each N:P ratio are referred to as 10, 15, and 20, while NP formulations with PA-siRNA (siPA-NPs) at each N:P ratio are referred to as 10 PA, 15 PA, 20 PA.

For *in vivo* preparations, NPs formed in dilute solutions at pH 7.4 were then concentrated to desired dosages using 15 mL Amicon spin filters, 50k MWCO, with one additional wash step in PBS −/− (to remove buffer salts and ensure appropriate osmolarity prior to injection). Prior to complexation, polymer and buffer solutions were sterile-filtered.

Formulated si-NPs and siPA-NPs were then evaluated for size and surface charge using a Zetasizer Nano ZS (Malvern Instruments, Worcestershire, UK). For encapsulation efficiency studies, a Quant-iT Ribogreen assay (Thermo Fisher, Waltham, MA) was used according to manufacturers' instructions, with polyplexes formulated at 100 nM siRNA. Unencapsulated siRNA was used for controls. For supplemental size evaluations in heparin and bovine serum albumin (BSA) conditions, polyplexes were formulated in pH4 buffer initially at 1 mg/mL and created as described above. Formulations were then incubated for 10 min with 40 U/mL heparin or 50 wt% (of the total polymer amount) BSA, and their size was evaluated using the Zetasizer Nano ZS.

2.5. pH-dependent hemolysis

To evaluate pH-responsiveness of NPs, a red blood cell hemolysis assay was used; the methods have been thoroughly described in our previous work [39,48].

2.6. NP stability

To evaluate polyplex stability, a Förster Resonance Energy Transfer (FRET) method was used. Fluorescently-labeled dsDNAs (5' fluorophores) containing Alexa-546 and Alexa-488 probes on the antisense strands, were co-encapsulated in NPs at equimolar amounts. The NPs were formulated at 100 nM, and challenged with either heparin sulfate (100, 40, 2 U/mL) or FBS (10%, 30%, 50%) in a black, clear bottom 96 well plate. Fluorescence intensity at 514 nm and 572 nm was measured using a plate reader (Tecan Infinite F500, Mannedorf, Switzerland). Fluorophores were excited at 488 nm. The FRET ratio was calculated as the ratio of emission signal at 572 nm to that at 514 nm.

2.7. Endotoxin

P(MPC-*bl*-(DMAEMA-*co*-BMA)) polymers were tested for endotoxin contamination using a Chromogenic LAL Endotoxin Assay Kit (GenScript, Piscataway, NJ). The instructions in the kit protocol were followed exactly with testing done at 3 mg/mL polymer.

2.8. In vitro knockdown, uptake, viability in MDA-MB-231 cells

For *in vitro* luciferase knockdown assays, MDA-MB-231 cells were transduced with the luciferase gene in a manner previously described [11]. Cells were then seeded at 2000 per well in black, clear-bottom 96-well plates. After allowing cells to adhere for 24 h, si-NPs and siPA-NPs were introduced into cell media at a concentration of 100 nM siRNA (against luciferase or scrambled control sequences). Treatments were removed after 24 h of incubation, and cell bioluminescence was then measured on an IVIS Lumina III imaging system (Caliper Life Sciences, Hopkinton, MA) at 24 h and 48 h after treatment by addition of 150 μg/mL luciferin. Luminescence was normalized to that of scrambled siRNA NP controls. Cell viability was measured by comparing luminescence of scrambled controls to untreated cells.

Cell uptake was measured after seeding normal, non-luciferase expressing MDA-MB-231 cells at 80,000 per well in 12-well plates (working volume 1 mL). The cells were allowed to adhere for 24 h, and 100 nM NP treatments were applied (Cy5-labeled). After 24 h, media was removed, and the cells were trypsinized, pelleted, and resuspended in PBS (−/−). Intracellular NP levels were measured by FACS (BD LSRII, Franklin Lakes, NJ), and data were quantified using FlowJo (Ashland, OR).

2.9. Intravital microscopy, biodistribution

Anesthetized male CD-1 mice (Charles River) were placed on the stage of a confocal microscope (Nikon Czsi + with Nikon Eclipse Ti-oE inverted microscopy base, Plan ApoVC 20X differential interference contrast N2 objective, 0.75 NA, Galvano scanner, 543 dichroic mirror). The ear of the mouse (hair removed) was placed on coverslip glass and immobilized with immersion oil. The microscope was focused onto prominent ear veins until red blood cell flow was clearly visible. Mice

were then injected with Cy5-NPs at 1 mg/kg dose via the tail vein; intravital fluorescence was monitored (imaging once per second) immediately prior to injection and for 30 min after injection or until the Cy5 signal reached half of its initial intensity (if longer than 30 min). Curve-fitting was performed using nonlinear regression in Graphpad Prism. Single phase and two-phase exponential decay models were considered and compared using Akaike's Information Criterion.

Mice (n = 5 per group) were sacrificed 24 h after injection, and organs were imaged for Cy5 (excitation 620, emission 670, auto exposure) fluorescence (total radiant efficiency) using the IVIS imaging system described above. All data were quantified using the Living Image Software (Perkin Elmer).

2.10. Toxicity studies in vivo

Female BALB/c mice (4–6 weeks, Charles River, Wilmington, MA), were enrolled in either a 6-injection study (n = 5 per group) or 3-injection study (n = 5–6 per group). For the 3-injection study, mice were injected by tail vein on day 1, 4, and 7 with NPs prepared as described above with 1 mg/kg siRNA. The mice were sacrificed 12 h after the final day 7 injection by cardiac puncture under isoflurane anesthesia. Blood and organs were harvested for further analysis (detailed below). Mouse body weight was recorded daily throughout the treatment period. For the 6-injection study, mice were injected on days 1, 4, 7, 14, 21, and 28. Mice were sacrificed 12 h after the day 28 injection. Additional mice (n = 5 per group) were injected subcutaneously once with LPS (50 μg) or CCl_4 (1:7 v/v in olive oil, 4 mL/kg) as positive controls for toxicity readouts. These mice were sacrificed 12 h after injection.

2.11. Serum markers and complete blood counts (CBCs)

For serum, CBC, and cytokine measurements, blood was harvested by cardiac puncture and collected in EDTA-coated tubes. Plasma was isolated by centrifuging blood samples at 3000 × *g* for 10 min and taking the supernatant. Complete blood counts, as well as plasma alanine aminotransferase (ALT), aspartate aminotransferase (AST), and blood urea nitrogen (BUN) were measured by the Vanderbilt Translational Pathology Shared Resource. Clinical chemistry testing was performed using the Alfa Wasserman ACE Alera system. Cytokines were measured by the Vanderbilt Hormone and Analytical Services Core using Multiplex Luminex technology (https://www.vumc.org/hormone/luminex).

2.12. Histology

Upon sacrifice, mouse tissues were collected, preserved in 10% formalin, and submitted to the Vanderbilt Translational Pathology Shared Resource, where they were embedded in paraffin, sectioned into 5 μm sections, and stained with hematoxylin and eosin (H&E). H&E stained slides were processed and scanned by the Vanderbilt Digital Histology Shared Resource (www.mc.vanderbilt.edu/dhsr). Slides were evaluated for toxicity-associated tissue damage by Dr. Kelli Boyd, DVM, PhD, DACVP and Dr. Lauren Himmel, DVM, PhD in the Vanderbilt Translational Pathology Shared Resource.

2.13. Liver immune cell analysis

Mice in the 6-injection study were sacrificed 12 h after final injection, and their livers were removed and stored in media on ice (less than 3 h). Livers were cut into small pieces and macerated through a 0.45 μm cell filter. Hepatocytes were allowed to settle for 20–30 min. Cells remaining in suspension were centrifuged for 5 min at 300 × *g*. Pelleted cells were resuspended in HBSS, underlayed with ISOLYMPH, and centrifuged at 300 × *g* for 30 min. The buffy coat was collected, pelleted, and resuspended in FACS buffer (1X PBS + 0.05% FBS + 0.1% NaN_3 + 0.02% EDTA) for staining.

Cells were stained using antibodies reactive against B220 (FITC, RA3-6B2), F4/80 (PE, BM8), CD5 (BV421, 53–7.3), Ly6G (PCPCy5.5, 1A8), CD11b (PECy7, M1/70), and AlexaFluor 700 succinimidyl ester to exclude dead cells. Antibodies were purchased from BD Biosciences, eBioscience, or Tonbo Biosciences. Samples were fixed with1X PBS + 1% paraformaldehyde (in 1X PBS) and run on a BD Biosciences LSRII flow cytometer. Data analysis was performed using FlowJo software (FlowJo LLC, Ashland, OR). Data are represented as percent of immune cells to account for differences in total cell numbers isolated from the buffy coat.

2.14. Anti-phosphocholine immunogenicity

In order determine whether repeat injection caused carrier-associated immunogenicity, serum of mice treated with 15 PA and 20 PA formulations was assayed for anti-phosphocholine antibodies. We first added 50 μL P(MPC-bl-(DMAEMA-*co*-BMA)) polymer solution (5 mg/mL in ethanol) into each well of a Nunc MaxiSorp plate (Thermo Fisher). Plates were allowed to dry completely overnight at room temperature. Blocker BSA (200 μL, Thermo Scientific), diluted to 1X in water, was then added to wells and incubated for 1 h at room temp. Wells were then washed three times with washing buffer (N503, Thermo Fisher). Plasma from Balb/c mice (n = 5) injected with the 6-injection protocol (described above) with siPA-NP formulations of 15 PA or 20 PA was then diluted 1:100 in PBS (−/−), added into the wells (100 μL), and incubated for 1 h at 37 °C. Serum positive for anti-phosphocholine and serum negative for anti-phosphocholine from the Mouse Anti-Phosphocholine IgG ELISA kit (Alpha Diagnostic International, San Antonio, TX, USA) were used as positive and negative controls. Wells were then washed five times with washing buffer, and 100 μL of HRP-conjugated antibody (0.2 μg/mL, goat anti-mouse, IgG, IgM H + L) was added to each well and incubated at room temperature for 1 h. The plate was then washed five times again with washing buffer. A 1-step slow TMB-ELISA (Thermo Fisher) was then incubated in the wells for 15 min in the dark. The colorimetric reaction was stopped using Stop Solution (N600, Thermo Fisher). Absorbance was measured at 450 nm, and absorbance values were normalized to measurements on the negative control serum to determine whether treated animal sera were positive for anti-phosphocholine antibodies.

2.15. Tumor studies

Athymic nude mice (Jackson Laboratories, Bar Harbor, ME, USA), were injected orthotopically in bilateral mammary fatpads with 1e6 luciferase-expressing MDA-MB-231 cells in a 50:50 mixture of Matrigel: serum-free DMEM). Tumor growth was monitored until tumors reached 100 mm^3, at which point mice were injected intravenously with 1 mg/kg siRNA packaged in either siPA-NPs (15 PA formulation, n = 19 tumors) or in *in vivo*-JetPEI (n = 10 tumors). Each formulation was prepared bearing either luciferase or scrambled siRNA sequences. In vivo Jet PEI was prepared according to optimized manufacturer's protocols (0.16 μL *in vivo*-JetPEI per μg siRNA). Tumor luminescence was measured and quantified using an IVIS Lumina III imaging system prior to injection and 24 h after treatment following injection of 150 mg/kg luciferin subcutaneously. For analysis, luminescence of each tumor at 24 h was compared to baseline luminescence for that tumor at 0 h. Values for tumors receiving luciferase siRNA treatment or PBS were then normalized to the average of tumors receiving scrambled siRNA.

For tumor biodistribution studies, athymic nude mice bearing MDA-MB-231 tumors (prepared as described above) were injected intravenously with either siPA-NPs or *in vivo*-JetPEI formulations (described above), bearing Cy5-labeled oligonucleotides (n = 4–6 tumors per group). The tumors were then excised from the mice, minced, and incubated for 1 h with rotation in media containing 0.5 mg/mL collagenase, 0.19 mg/mL DNase. Tumors cells were then resuspended in HBSS (−/−), incubated in 5 mM EDTA for 20 min, filtered through a

70 μm strainer, washed in HBSS (+/+), immersed in ACK lysis buffer for 2 min, washed and resuspended in PBS (−/−), and measured for Cy5 fluorescence using a BD Biosciences LSR II cytometer in the Vanderbilt Flow Cytometry Shared Resource.

2.16. Statistical methods

All statistical tests were performed using either one-way ANOVA with multiple comparisons test (in cases of two or more groups) or two-tailed student's t-test (in comparisons with only 2 groups) with $\alpha = 0.05$. *In vivo* tumor knockdown data was analyzed using a non-parametric Kruskal-Wallis test with Dunn's multiple comparisons test. Data are displayed as mean plus standard error.

2.17. Ethics statement

All animal experiments described herein were carried out according to protocols approved by Vanderbilt University's Institutional Animal Care and Use Committee, and all studies followed the National Institutes of Health's guidelines for the care and use of laboratory animals.

3. Results and discussion

3.1. Synthesis of polymers and PA-Conjugated siRNA

The P(MPC-*bl*-(DMAEMA-*co*-BMA)) diblock co-polymers were successfully synthesized by RAFT polymerization with controlled molecular weight. The core block of these polymers comprised a degree of polymerization (DP) of 156, with a 50:50 monomer composition of DMAEMA:BMA and polydispersity (PDI) of 1.02 as determined by ^{1}H NMR and gel permeation chromatography (Supplemental Fig. 1). This core block monomer ratio was previously shown to optimally balance cytocompatibility with siRNA packaging, endosomal escape properties, and bioactivity [39]. The P(MPC) hydrophilic block was then polymerized from the p(DMAEMA-*co*-BMA) macroCTA with a DP of 67 (19.8 kDa) as confirmed by ^{1}H NMR (Supplemental Fig. 1). NPs with ~20 kDa molecular weight P(MPC)-based coronas were shown previously to extend circulation time compared to shorter PEGs and improve *in vivo* tumor cell uptake compared to high molecular weight PEGs [11].

The hydrophobized siRNA used in this work was synthesized by conjugating NHS ester-modified PA to amine-modified sense strand of the siRNA. Due to the molar excess of PA used in the reaction, the formation of the PA-conjugated siRNA (PA-siRNA) conjugate was highly efficient, with unmodified siRNA peaks undetectable by HPLC in the final product (data not shown). The molecular weight of the single-stranded, PA-siRNA was confirmed by LC-MS-ESI ($m/z = 8566$ for scrambled-sequence siRNA, expected MW = 8565 g/mol).

3.2. Formulation and pH-Responsiveness of NPs

We formulated 6 unique NP samples using either normal siRNA (si-NPs) or PA-modified siRNA (siPA-NPs) at N:P ratios of 10, 15, 20 (Fig. 1). These formulations are indicated throughout this work as 10, 15, 20, 10 PA, 15 PA, and 20 PA. For all studies, the dose of siRNA was kept constant, only changing the amount of polymer. Despite the different amounts of polymer utilized, the hydrodynamic diameter of all formulations was similar at approximately 100 nm (Fig. 2A), and all zeta potentials were close to 0 mV (Fig. 2B). Other studies that have explored the impact of N:P ratio on NP performance have mostly done so in the context of PEI or PEG-PEI-based polyplexes, where a change in N:P ratio causes a significant change in surface charge of the polyplex [23,32,33,36,49]. Because size and surface charge can significantly alter NP biodistribution [20], this polyplex formulation library is advantageous in that it enables exploration of the impact of N:P ratio without confounding changes in size or surface charge. The consistent size and zeta potential of the candidate NPs is likely dictated by the relatively high molecular weight, super-hydrophilic P(MPC) corona-forming polymer that forms stable, neutrally-charged NPs with high resistance to serum protein or complement adsorption [11].

At N:P ratios of 10, 15, or 20, all formulations maintained 70–80% encapsulation of siRNA (Fig. 2C). However, at lower N:P ratios of 1 or 5, siPA-NPs had significantly higher encapsulation efficiencies than si-NPs. The siPA-NPs with dual hydrophobization on the carrier polymer and cargo siRNA, therefore, more efficiently encapsulate siRNA at lower N:P ratios, likely due to hydrophobic carrier-cargo interactions and/or hydrophobicity-driven clustering of PA-siRNA molecules. However, encapsulation efficiency was consistently high for the 6 formulations used in this work at N:P ratios of 10,15, and 20, regardless of hydrophobization of the siRNA.

The ability to trigger endosomal rupture and escape is a necessary carrier property to ensure siRNA access to the cell cytoplasm where it is active. The pH-dependent membrane disruptive activity of the P(MPC-*bl*-(DMAEMA-*co*-BMA)) polymers was characterized for each formulation using a red blood cell hemolysis assay (Fig. 2D), which simulates endosomolysis [48]. At physiological pH, no formulations exhibited significant hemolytic activity, an indicator of their safety in circulation. However, all formulations exhibited strong hemolytic activity at pH 6.8 or lower, indicating their ability to disrupt endosomal membranes in response to a pH drop within endolysosomal vesicles. Neither the N:P ratio nor the presence of palmitic acid on the siRNA significantly altered the pH-dependent hemolytic behavior, which is driven by the polymer.

3.3. In vitro knockdown and cytotoxicity of NPs

Prior to *in vitro* cell assays, the P(MPC-*bl*-(DMAEMA-*co*-BMA)) polymers used for NP formulation were tested for endotoxin. Endotoxin is a potent stimulator of innate immunity and can have significant effects on both *in vitro* and *in vivo* toxicology, independent of the NPs themselves. No endotoxin contamination was found in the P(MPC-*bl*-(DMAEMA-*co*-BMA)) polymers (Supplemental Fig. 2A).

In vitro, all formulations were well-tolerated with low cytotoxicity up to 150 nM siRNA in MDA-MB-231 cells (Fig. 2E). At 100 nM, average viability ranged from 88 to 95%. At higher doses of polymer and siRNA, NP toxicity increased. At these higher doses (200–300 nM siRNA), NP toxicity was positively correlated with N:P ratio, indicating that polymer itself (as opposed to the siRNA) was the source of cytotoxicity since the amount of polymer increased with increasing N:P ratio while siRNA dose was held constant at a given dose level. This trend was present regardless of dual hydrophobization state. At each dose, there were no significant differences between cytotoxicity of si-NPs vs siPA-NPs. After removing NP treatments and waiting 24 h, cell viability recovered rapidly for all doses up to 300 nM siRNA (Supplemental Fig. 2B). Our data suggest that in an *in vitro* environment, the addition of PA-siRNA did not significantly impact viability. The reduced cell viability at higher N:P ratios highlights the need for reducing polymer dose to achieve non-toxic NP formulations, particularly since DMAEMA, like most cationic polymers involved in nucleic acid delivery, is known to be cytotoxic at high concentrations [21].

Each si-NP and siPA-NP formulation was next tested for *in vitro* bioactivity by knocking down the model gene luciferase in MDA-MB-231 cells (Fig. 2F). The amount of luciferase knockdown positively correlated with the relative amount of polymer (increasing N:P ratio) in the NP formulation at both 24 and 48 h after treatment. By 48 h, NP formulations at 20 or 20 PA achieved 93–97% silencing, while formulations at 10 or 10 PA exhibited average silencing of 50%–70%. Similar to the cell viability results, the presence of PA in the formulations did not significantly alter the silencing efficiency *in vitro*. Uptake of fluorescently-labeled NPs was also measured for each formulation (Supplementary Fig. 2C). Interestingly, while all formulations exhibited

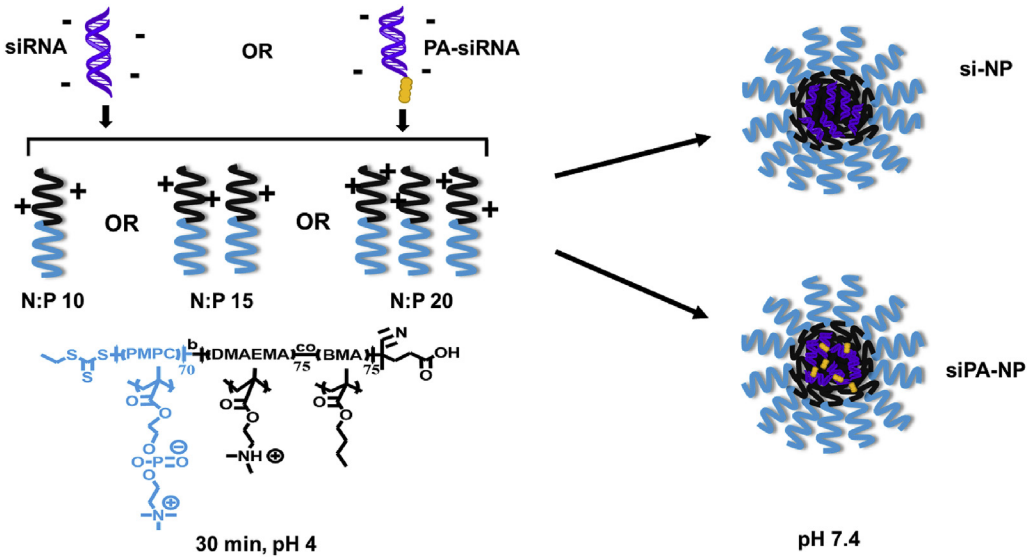

Fig. 1. Formulation of si-NPs and siPA-NPs. The NPs were made at N:P ratios of 10,15, and 20 with either un-modified siRNA, or hydrophobically-modified PA-siRNA. To form NPs, siRNA was complexed with P(MPC-*bl*-(DMAEMA-*co*-BMA)) polymers at pH 4 for 30 min, and then pH was raised to 7.4.

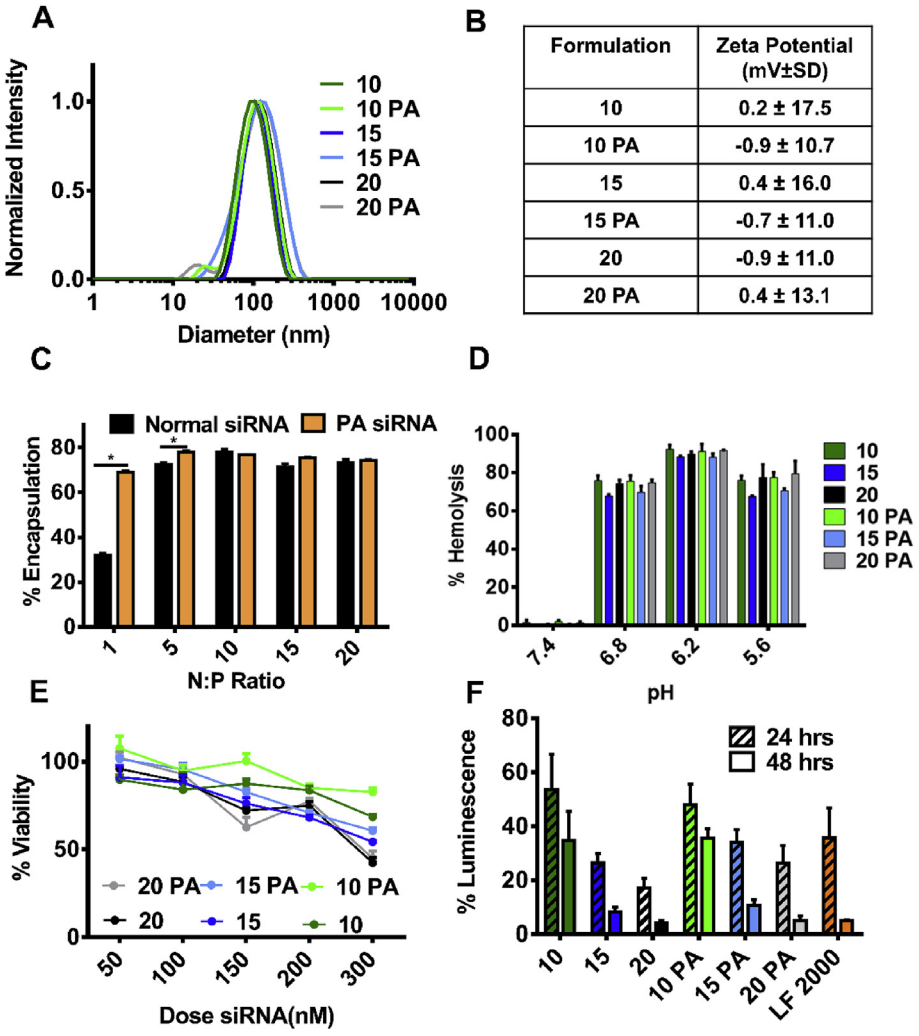

Formulation	Zeta Potential (mV±SD)
10	0.2 ± 17.5
10 PA	-0.9 ± 10.7
15	0.4 ± 16.0
15 PA	-0.7 ± 11.0
20	-0.9 ± 11.0
20 PA	0.4 ± 13.1

Fig. 2. Characterization of NP size, charge, pH-dependent membrane disruption activity (marker for endosome escape), siRNA encapsulation efficiency, *in vitro* viability, and activity. (A) All NP formulations were approximately 100 nm in diameter and (B) had neutral zeta potentials. (C) The siPA-NPs exhibited increased encapsulation efficiency at low N:P ratios relative to si-NPs based on Ribogreen quantification at 100 nM siRNA doses ($n = 3$, $p < 0.05$). (D) All NPs display pH-dependent membrane disruption tuned to cause lack of toxicity (no hemolysis at pH 7.4) and endosome disruption (hemolysis at pH 6.8 and below) at 40 μg/mL polymer. (E) Viability of MDA-MB-231 cells 48 h after exposure to NP formulations at siRNA concentrations from 50 to 300 nM. (F) *In vitro* knockdown of luciferase in MDA-MB-231 cells 24 and 48 h after siNP exposure at 100 nM siRNA. Increasing N:P ratio increased *in vitro* knockdown, but addition of PA-siRNA had no significant effect.

significantly increased uptake compared to commercial Lipofectamine 2000, there were no significant differences in uptake caused by increasing N:P ratio, which is consistent with the expected result based on these NPs all having similar diameter, zeta potential, and siRNA packaging efficiency. There was a small increase in average mean fluorescence for cells treated with siPA-NPs, but it was only significant at N:P 10. This result agrees with the bioactivity data which shows that addition of PA-siRNA did not significantly change gene knockdown. However, NPs formulated at different N:P ratios had different levels of bioactivity despite achieving similar level of cell internalization, suggesting that increasing N:P ratio may improve bioactivity by mechanisms other than uptake, such as increased endosomolytic properties that are not sensitively measured by *in vitro* hemolysis assays. This result is consistent with earlier work utilizing PA-siRNA in PEGylated si-NP systems [13]. *In vitro,* it was expected that the stability advantages imparted by PA-siRNA would be less apparent, since there is a low percent serum (10% in these studies), a lack of competition by molecules such as proteoglycans, and a hemodynamically static environment with reduced mechanical and dilution concerns. It was anticipated that PA-siRNA may impart stability differences that are more impactful *in vivo* and that could alter the stability (which has impacts on toxicity), systemic circulation, and tissue accumulation/activity of NPs.

3.4. Stability of NPs

Two of the major challenges to NP stability in circulation are serum proteins and anionic heparan sulfate proteoglycans in the kidney glomerular basement membrane [18,20]. In order to understand the potential impact of N:P ratio and hydrophobized siRNAs on NP stability *in vivo*, we challenged NPs with various concentrations of serum and heparin in a FRET-based assay (Fig. 3). This assay involves co-encapsulation of FRET-paired siRNAs, and an increased FRET ratio indicates better siRNA encapsulation stability.

With both heparin and serum challenge, increasing N:P ratio increased stability, particularly at low challenge concentrations, while siRNA conjugation with PA was increasingly important to stability at high challenge concentrations. In heparin at 100 U/mL and 40 U/mL, 20 PA formulations consistently had the highest average stability, while formulations at N:P 10 with normal siRNA consistently had the lowest average stability, as determined by FRET ratio (Fig. 3A and B). The 15 PA NPs had the second highest stability, while 15, 20, and 10 PA formulations all displayed similar FRET ratios throughout 60 min and were not significantly different from each other. These data suggest that with increased concentration of heparin, siRNA conjugation to PA significantly improves resultant NP stability, particularly at higher N:P ratios. At 2 U/mL of heparin, the effect of N:P ratio on stability was predominant, with polyplexes formulated at 20 significantly more stable than those formed at 15 or 10 (Fig. 3C). Thus, at lower concentrations of heparin, NP stability is significantly increased by increasing N:P ratio, while siRNA conjugation to PA had a relatively negligible effect for each individual N:P ratio.

In 50% or 30% serum, 15 PA and 20 PA once again exhibited the

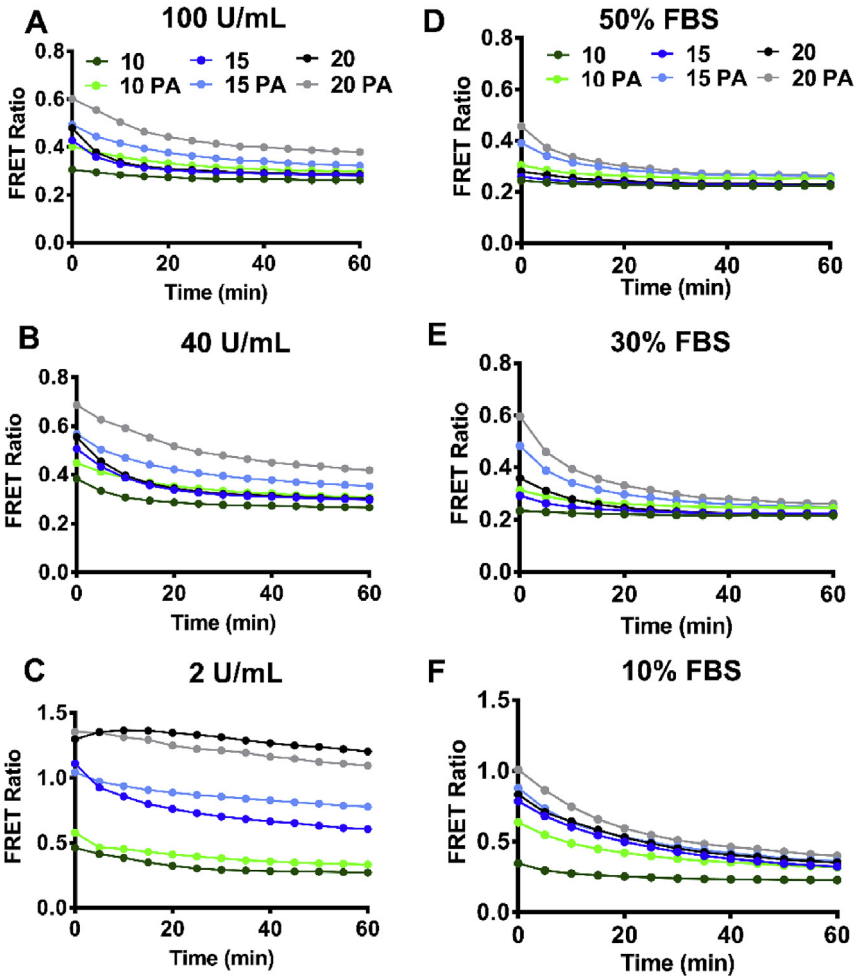

Fig. 3. Stability of NPs over time in FBS and anionic heparin sulfate is dependent on both N:P and dual hydrophobization. (A–C) NPs at 100 nM siRNA were exposed to 100, 40, or 2 U/mL heparin or (D–F) 10,30, or 50% FBS, and the ratio of fluorescence at 572 nm–512 nm was measured. In general, NPs at higher N:P ratios or that were made with PA-siRNA displayed increased cargo loading stability.

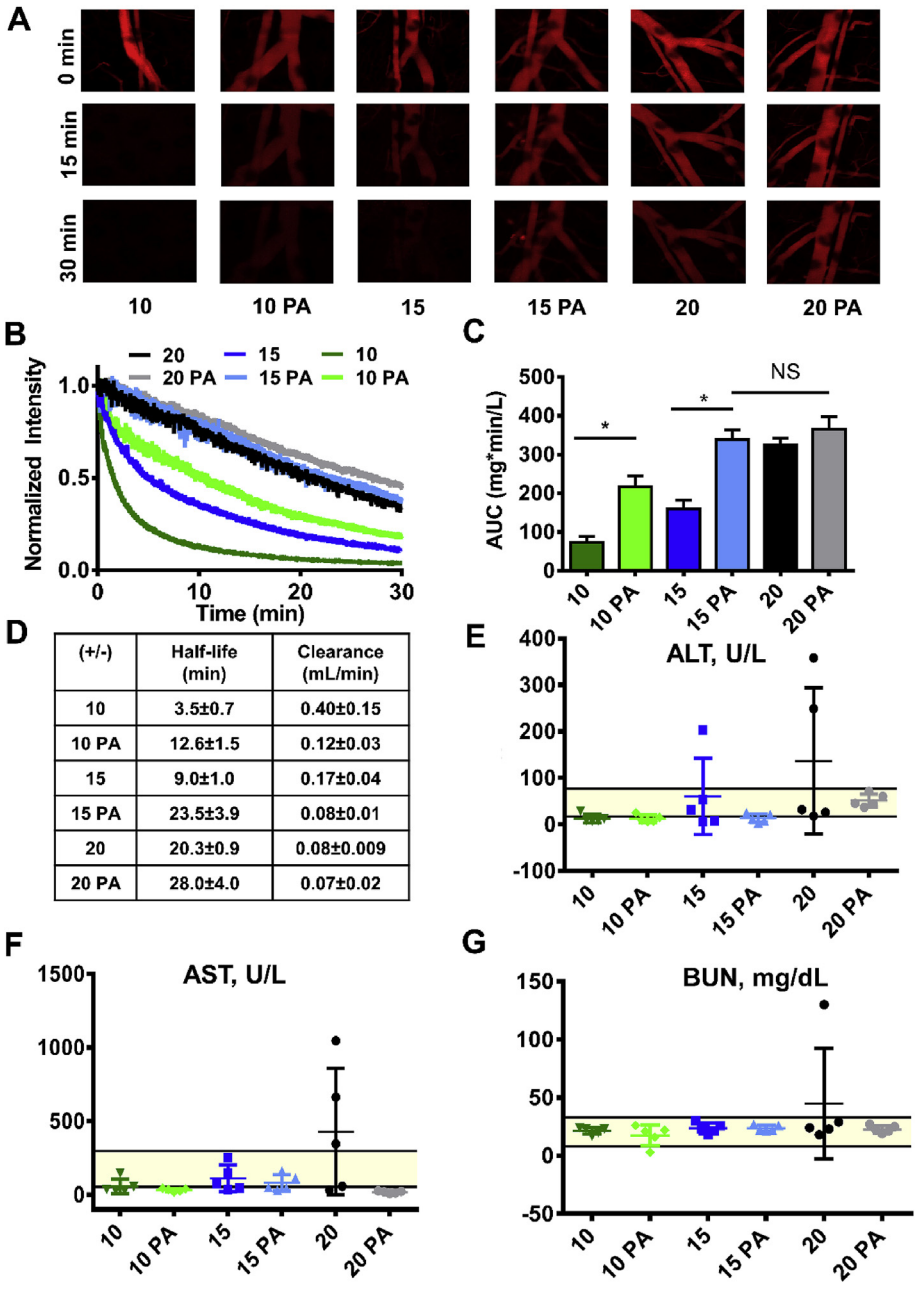

(+/-)	Half-life (min)	Clearance (mL/min)
10	3.5±0.7	0.40±0.15
10 PA	12.6±1.5	0.12±0.03
15	9.0±1.0	0.17±0.04
15 PA	23.5±3.9	0.08±0.01
20	20.3±0.9	0.08±0.009
20 PA	28.0±4.0	0.07±0.02

Fig. 4. Interplay of N:P and dual hydrophobization impacts *in vivo* pharmacokinetics and toxicology. (A) Representative intravital microscopy images of Cy5-siNPs in the mouse ear. (B) Average pharmacokinetic curves (first 30 min) for each NP formulation, normalized to initial fluorescence intensity (n = 5). (C) Increasing N:P ratios and addition of PA-siRNA at N:P 10 and 15 significantly increased NP area under the curve ($p < 0.05$, n = 5). (D) Table of half-lives and clearance values for each NP formulation. Longest half-lives were achieved by siPA-NPs formulated at 20 PA. (E–G) ALT, AST, and BUN sampled from blood sera collected at 24 h after a single injection of NPs show toxicities dependent on polymer dose in the N:P 20 and N:P 15 groups (n = 5). Toxicities were abrogated in NPs formulated with PA-siRNA. Horizontal y-axis lines indicate normal mouse plasma ranges for ALT, AST, and BUN.

highest FRET ratios, indicating their increased stability (Fig. 3D and E). Here again, in higher serum conditions, siRNA conjugation to PA increased FRET ratios compared to the si-NPs without dual hydrophobization at equivalent N:P ratios. At 50% serum, all siPA-NPs had higher FRET ratios, while si-NPs at all N:P ratios tested without PA-siRNA exhibited equally low stability, and their FRET traces were not significantly different from each other. At lower serum conditions (10% FBS), the impact of N:P ratio was more apparent, as NPs at 15 and 20 had consistently higher stability than NPs formulated at N:P 10, although 20 PA NPs were still the most stable, with significantly greater FRET ratio than the si-NPs at N:P 10 after 1 h of serum exposure (Fig. 3F). Incubation of all NP formulations in 40 U/mL heparin or bovine serum albumin did not significantly impact particle size (Supplemental Fig. 3). Together, these data suggest that formulating NPs at higher N:P ratios can improve their stability against serum or heparin at lower concentrations, but addition of dual hydrophobization (in siPA-NP formulations) is more effective for increasing stability at higher serum or heparin levels representative of the *in vivo* environment.

3.5. *In vivo* pharmacokinetics si-NP and siPA-NP formulations

We next explored the impact of N:P ratio and dual hydrophobization on *in vivo* NP pharmacokinetics using intravital microscopy (IVM) of the mouse ear vasculature. Each formulation bearing fluorescently-labeled siRNA was injected intravenously and tracked via confocal microscopy (representative images in Fig. 4A). Electrostatically-complexed particles historically have more rapid blood clearance than solid nanoparticulate systems. IVM allows for more accurate measurement of NP clearance and early-phase half-lives because it enables continuous sampling of fluorescent signal, starting immediately after injection.

Overall, increasing N:P ratio significantly increased NP area under the curve and circulation half-life (Fig. 4B–D). The si-NPs formulated at 15 and 20 had half-lives increased by 2.5-fold and 5.7-fold respectively compared to si-NPs formulated at N:P 10, ranging from 4 min (N:P 10) to 9 min (N:P 15) to over 20 min (N:P 20). At N:P 20, AUC was

significantly increased by over four-fold compared to N:P 10, and two-fold compared to N:P 15. Similarly, average clearance for si-NPs formulated at N:P 20 was significantly lower than either formulations at 10 or 15. Thus, increasing the amount of polymer relative to siRNA significantly improved pharmacokinetic characteristics.

Dual hydrophobized siPA-NPs had enhanced area under the curve and circulation half-lives relative to si-NPs, particularly at the lower N:P ratios. The siPA-NPs at N:P 10 and N:P 15 had a three-fold and two-fold, respectively, increase in area under the curve relative to the corresponding si-NPs at the same N:P ratios. At N:P 10, siRNA conjugation to palmitic acid nearly quadrupled average NP half-life. At N:P 15, dual hydrophobization increased half-life average from 9 min to 23.5 min. The benefits of dual hydrophobization begin to diminish at N:P 20, at which point addition of PA did not significantly increase half-life or area under the curve. Importantly, siPA-NPs formulated at 15 PA did not have significantly different area under the curves from either 20 or 20 PA NPs. Thus, addition of PA enables delivery of the same doses of siRNA with similar pharmacologic profiles (at 15 PA, 20, and 20 PA), but with a lower dose of polymer for the optimized 15 PA formulation.

Each of the NP formulations was determined to have first order, single-phase elimination kinetics, based on the best fit nonlinear regression analysis (curves shown in Supplementary Fig. 4A). This fit can also be demonstrated visually by the linearity of each elimination curve when plotted in log scale (Supplementary Fig. 4B). The one exception to this trend is the si-NPs formulated at N:P 10. Because these polyplexes are the least stable, it is likely that some of the Cy5-labeled nucleic acids were rapidly destabilized, and an early-phase elimination is visible for the free nucleic acid population.

Twenty-four hours after intravenous injection, the organ biodistribution for all NP formulations was similar, with greatest accumulation in the liver and kidneys (Supplemental Fig. 4C). Both 15 PA and 20 PA formulations had significantly lower fluorescence in the kidneys compared to si-NPs at N:P 20 with normal siRNA, which had the highest amount of kidney fluorescence. These data suggest that the dual hydrophobized formulations at higher N:P ratios are less prone to clearance by disassembly in the kidney glomerular basement membrane.

At 24 h after a single injection, mice treated with NPs formulated at higher N:P ratios (15, 20) with normal siRNAs showed signs of elevations above normal ranges in ALT, AST, and BUN, indicators of liver and kidney toxicity (Fig. 4E–G). In the si-NP N:P 20 group, 3/5 mice had above-normal AST, 2/5 had elevated ALT, and one had increased BUN. In the N:P 15 group, only one mouse showed any sign of abnormally high serum enzymes (ALT). However, addition of PA-siRNA in these formulations completely abrogated signs of toxicity; none of the mice treated with dual hydrophobized siPA-NPs experienced elevation in the serum toxicity markers measured.

The combined pharmacokinetic profiles and liver enzyme data suggest that dual hydrophobization strategies can impart significantly increased stability to electrostatically-complexed polyplexes in circulation while reducing toxicity associated with increased doses of polymer. We have shown that increasing N:P ratio significantly improves circulation half-life *in vivo*, but comes at a toxicologic cost associated with increased cation-containing polymer in the formulations. This toxicity is likely related to reduced stability and exposure of the cationic core polymer block, as free polycations are known to interact with circulating cells or serum components [25]. PA-modified siRNA increases the hydrophobic interactions between polymer and siRNA relative to unmodified siRNA, increasing NP stability and preventing premature exposure of the cationic moieties in the NP core to the exterior of cells (prior to entry into acidifying endosomes). Addition of PA-siRNA can therefore reduce the toxicity of high-polymer formulations and significantly increase the half-life of low-polymer formulations.

As we and others have demonstrated, increases in pharmacokinetic area under the curve typically correlate with significantly increased tumor biodistribution [12,13,50,51]. Tumor accumulations of nanomedicines is typically driven at least in part by the enhanced permeability and retention effect (EPR), which has been observed in solid tumors in human patients, and is known to positively correlate with intravenous area under the curve [50–52]. Extended siPA-NP circulation times may indicate reduced polyplex disassembly in the kidney and increased opportunity for passive accumulation of siRNA in target tissues.

It is rare for electrostatically-complexed polymeric NPs to have alpha-phase half-lives as long as those achieved by our high N:P ratio, dual-hydrophobized carriers. PEGylated polycations or emulsion-based cationic nanogels clear from circulation completely by 20 min [19,33]. Though some systems have utilized hydrophobic core monomers to improve stability of PEG-shielded, cationic carriers, first-phase circulation half-life is frequently less than 5 min due to a first-pass effect in the liver [53]. Even core disulfide crosslinking, as demonstrated by the Kataoka group, did not improve NP circulation half-life to longer than 5–10 min when introduced to polyion complex micelles [44,54,55]. When a cholesterol-modified siRNA was added, the half-life was modestly extended to over 20 min (single hydrophobization), further supporting the powerful impact of hydrophobization of siRNA on nanocarrier circulation [44]. Similarly, clinically studied CALAA-01 complexes utilizing guest-host cyclodextrin-adamantane stabilization of polymer components were completely cleared from circulation in 30 min in humans, probably due to rapid dissociation in the kidney [18].

To date, few studies have demonstrated the *in vivo* impact of small changes in N:P ratio on polyplex pharmacokinetics or toxicity. N:P ratio is most often explored in the context of encapsulation efficiency *in vitro*, with selection based on the lowest N:P ratio with adequate encapsulation of nucleic acid. However, in our case, NPs formulated at 10, 15, and 20 all had equally high encapsulation efficiencies and identical physicochemical properties (size, surface charge), yet produced markedly different *in vivo* pharmacokinetic properties. Notably, polymer dose has been demonstrated to improve *in vivo* stability in the context of various crosslinking strategies in PEGylated poly(L-lysine)-based NPs; the use of 2-iminothiolane crosslinking increased the ratio of polymer to siRNA and improved polyplex blood circulation compared to 3,3′-dithiobispropionimidate crosslinking, which resulted in lower polymer to siRNA ratios and lower stability [54]. Other groups have primarily studied N:P ratio in the context of how polyplex surface charge impacts organ biodistribution; it has often been observed that increasing N:P correlates with higher accumulation in the lung and rapid clearance from circulation, driven by increasing surface charge [33,49]. To our knowledge, our data are the first to comprehensively characterize the impact of charge ratio and dual hydrophobization on the pharmacokinetic profiles and toxicity of siRNA-containing NPs and to make the unique observations that dual hydrophobization can reduce the amount of polymer needed to achieve maximal AUC, while also reducing toxicity *in vivo* for a defined N:P ratio.

3.6. *In vivo* safety of NP formulations

Because many applications of siRNA therapeutics, including delivery to solid tumors, require repeated intravenous dosing of NPs, we further explored the impact of charge ratio and PA-siRNAs on more rigorous toxicologic parameters after multiple injections. Additionally, the effects of long-term administration of zwitterionic-corona NPs have thus far not been well-characterized.

We injected two cohorts of healthy BALB/c mice with 1 mg/kg NPs on different treatment schedules. In the first group, we injected NPs i.v. 3 times over the course of a week (3 injection course; day 1,4,7). In the second treatment group, we injected NPs i.v. 6 times over the course of a month (6 injection course; day 1,4,7,14,21,28). In both cases, the animals were sacrificed 12 h after the final injection. We performed a comprehensive panel of tests to determine the relative safety of the formulations, including assessing serum enzymes, complete blood

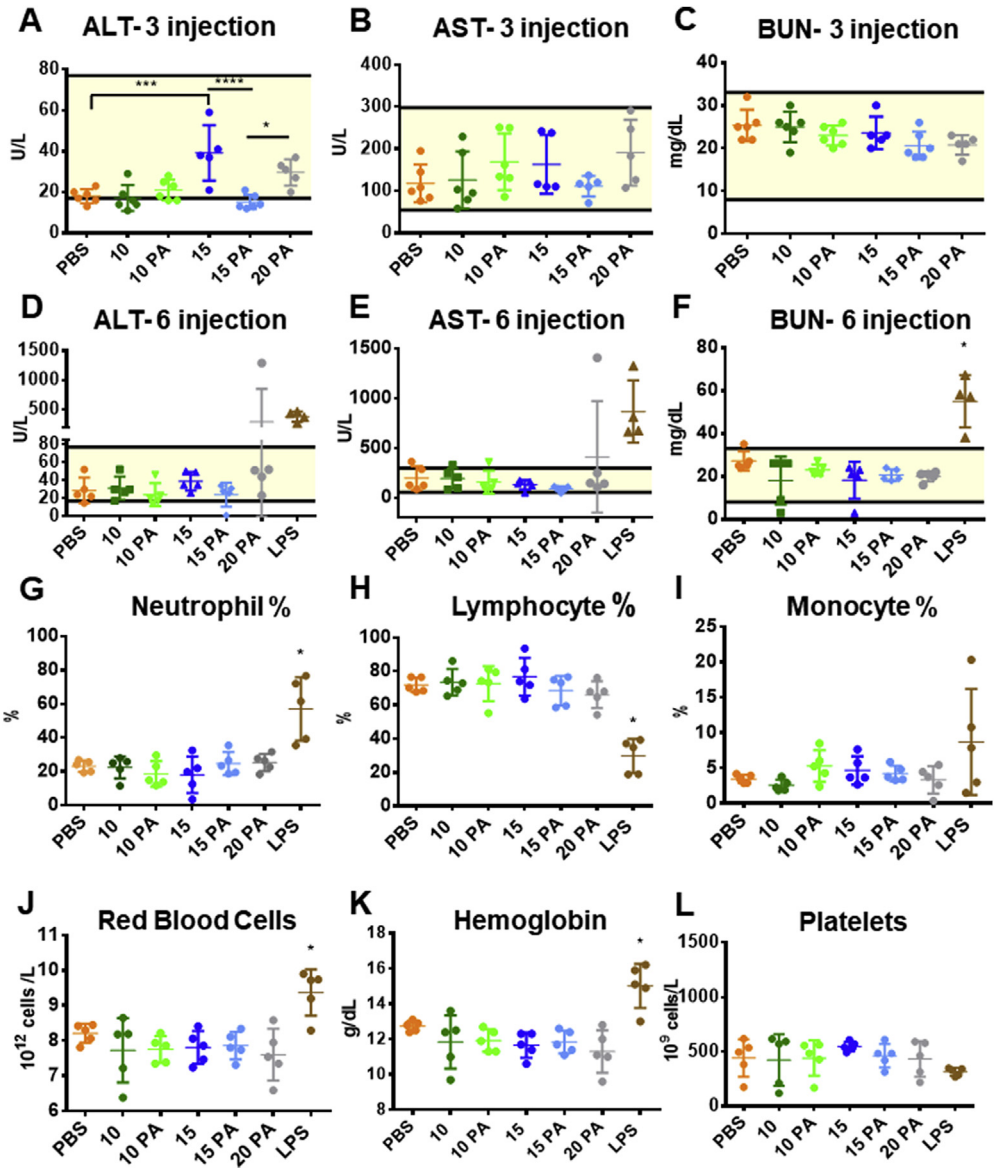

Fig. 5. All NPs tested had minimal toxicological effects under the multi-injection treatment courses. ALT, AST, and BUN levels in mice sera 12 h after the final injection of a 3-injection course (A–C) or 6-injection course (D–F) show that NPs were well-tolerated across multiple injections (n = 5–6). Y axis lines indicate normal ranges. The only detectable adverse elevations were in the 20 PA group after 6 doses of 1 mg/kg siPA-NPs over the course of 1 month. Mice treated with LPS were used as a positive control for liver and kidney damage. (G–L) Complete blood counts 12 h after the final injection of the 6-injection course show no abnormal changes in circulating lymphocytes, erythrocytes, or platelets, for any of the sampled NP formulations (n = 5–6). (For interpretation of the references to color in this figure legend, the reader is referred to the Web version of this article.)

counts, plasma cytokines, body weight, histology, liver immune cell content, and immunogenicity. Because of the trends toward acute toxicities observed 24 h after a single injection in the N:P 20 group, we limited our studies to formulations at 10, 15, 10 PA, 15 PA, and 20 PA. As a positive control for toxicity, another group of mice was injected with LPS once and sacrificed 12 h later. For both injection courses, no significant changes in body weight were noted for any of the mice receiving any NP formulation (Supplementary Fig. 5).

After the week-long, 3-injection course, there were no elevations in ALT, AST, or BUN outside of normal ranges, indicating that all formulations were well-tolerated (Fig. 5A–C). However, the ALT levels for N:P 15 group were significantly increased from saline-injected mice and from the 15 PA group ($p < 0.01$, n = 5–6), suggesting that addition of PA-siRNA reduced liver toxicity. The 20 PA group also had significantly higher ALT levels than the 15 PA group ($p < 0.03$, n = 5–6), suggesting some polymer dose-dependent effects in the liver. After the month-long, 6-injection course, all NP formulations remained within normal range except for one mouse in the 20 PA group, which experienced elevations in ALT and AST (Fig. 5D–F). This indicates that in the context of a multi-injection study, even with addition of PA-siRNA, higher N:P ratios may cause liver toxicity. Overall, there were no statistically significant differences between NP formulation groups and saline-treated groups after the 6-injection course. Thus, the relatively small ALT differences observed after the more frequent 3-injection in 1-week schedule are likely temporary elevations that were resolved after the month-long course.

The complete blood counts for all formulations were not significantly different from saline-treated mice for either the 3-injection (Supplemental Fig. 6A-I) or 6-injection courses (Fig. 6G-L, Supplementary Fig. 6J-L). Often, a concern with electrostatically-complexed NPs such as the clinically-studied CALAA-01, is that they may cause platelet aggregation in circulation, which reduces overall platelet count [24]. However, no significant changes in platelet counts were recorded for any of the tested NPs, indicating that the NPs in this study did not induce major platelet aggregation, regardless of N:P ratio. LPS treatment, on the other hand, induced significant decreases in % lymphocytes with corresponding increases in % monocytes, % neutrophils, red blood cell count, and hemoglobin. These data provide further support that the si-NPs and siPA-NPs at each N:P ratio tested were well-tolerated upon long-term, repeated administration.

None of the NP formulations tested in this study induced significant increases in cytokines that would indicate immunotoxicity (Fig. 6A–H). At 12 h after the final injection in the 3-injection course, one mouse in the N:P 15 group showed modest increases in IFNγ (Fig. 6A), and one

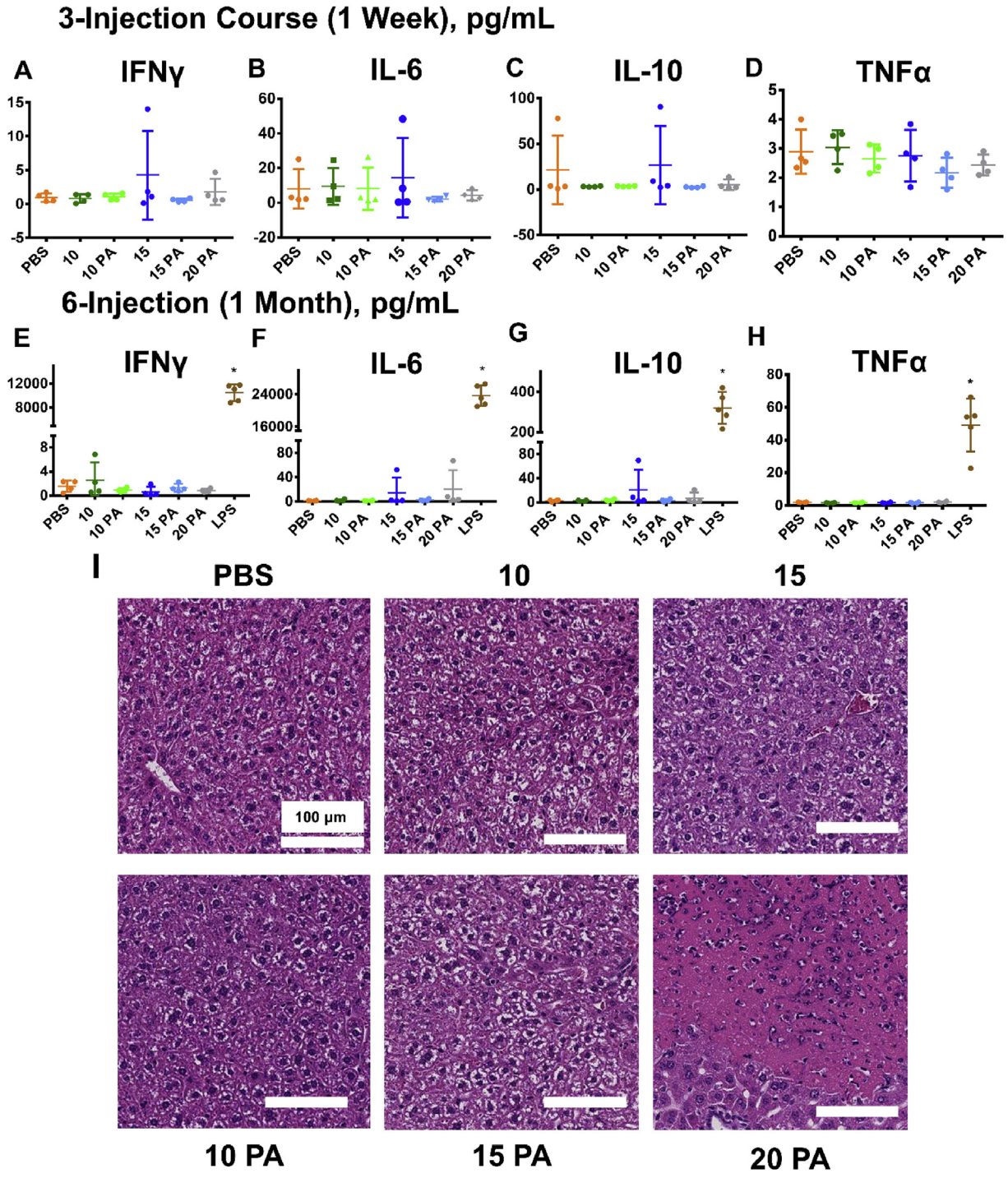

Fig. 6. Cytokines and liver histology associated with multi-injection courses. IFNγ, IL-6, IL-10, and TNFα sampled from serum of BALB/c mice 12 h after the final dose of a 3-injection course (A–D) or a 6-injection course (E–H) (n = 5). Compared to LPS-injected positive control mice, there were no significant or unsafe elevations in any cytokine levels measured. A few mice experienced cytokine increases after administration of NPs formulated at 15, which were notably the highest polymer dose tested without dual hydrophobization. (I) Representative liver histology after 6-injection course. For NPs formulated at 10, 15, 10 PA, or 15 PA, all livers were similar to saline treated mice or exhibited minimal signs of single cell or focal necrosis. However, at the highest polymer dose of 20 PA, 2/5 mouse livers had visible areas of focal necrosis.

mouse had increased IL-6 (Fig. 6B) (14- and 6-fold above the saline average, respectively). After the 6-injection course, one mouse in each of the 15 and 20 PA groups had slightly elevated IL-6 (Fig. 6F) (43 and 56-fold above the saline average), and the same mouse from the 15 group and a different mouse in the 20 PA group had elevated IL-10 (Fig. 6G) (26-fold and 8-fold above the saline average, respectively). The increase in IL-10 in these groups after longer-term injections matches evidence from the CALAA-01 studies, in which continuous polyplex dosing increased the serum levels of the anti-inflammatory cytokine IL-10 [56], perhaps a compensatory mechanism against carrier-related effects. However, all cytokine increases were modest compared to the LPS-treated mice, which were on the order of hundreds to thousands-fold greater than the saline averages. The siRNAs used in this study contained multiple O-methyl modifications to reduce their

potential immunostimulatory effects, so any cytokine increases are likely caused by polymer components of the NP formulations. In our study, only the NP formulation containing either the highest polymer dose (20 PA) or the highest polymer dose without hydrophobized siRNAs (N:P 15), induced slight cytokine responses, further suggesting that any immunostimulation is dependent on overall polymer dose and NP stability. Overall, our data indicate that the zwitterionic NP formulations were well tolerated over long-term, repeated administration.

Liver, spleen, lung, and kidney tissues were evaluated for histological abnormalities by blinded veterinary pathologists after completion of each injection course. In the 3-injection course, all tissues were determined to be "unremarkable" (data not shown). For the 6-injection course, spleen, lung, and kidney tissues were also determined "unremarkable" (Supplemental Fig. 7A and B). Mouse livers were graded for signs of necrosis, with most NP treated mice showing normal histology (Fig. 6I). However, in the livers of mice in the 20 PA group, there were detectable areas of coagulation necrosis in 2 out of 5 mice. One mouse in the 15 PA group showed evidence of a very small area of coagulation necrosis (Supplementary Fig. 7C). The livers of two mice each in the 15 PA and 15 groups had only 1–2 single necrotic cell foci, while 4/5 mice in the 20 PA group had signs of single cell necrosis (Supplemental Fig. 8A). All cases of cellular necrosis in these mice were therefore very small, with clinically relevant amounts of necrosis occurring in only one of the 20 PA treated mice, which aligns well with serum liver enzyme results (Fig. 5D and E). In the livers of mice treated with a positive control for liver toxicity, carbon tetrachloride (CCl_4), necrosis was more widespread (Supplemental Fig. 8B). The histologic analysis therefore indicates that while all formulations were relatively well-tolerated, repeated injection of many doses at the "high polymer" 20 PA condition could result in some minor but likely manageable liver damage. In sum, we observed a clear polymer dose dependence for liver injury, which highlights the need to reduce overall polymer dose while maintaining optimal pharmacokinetic properties of NP formulations.

Based on our liver histology results, we also characterized the populations of immune cells present in the livers of mice subjected to the 6-injection course to test for an inflammatory response by innate immune cells. While mice treated with the liver-toxic agent, CCl_4, experienced elevations in percentages of liver macrophages and neutrophils, none of the NP formulations significantly altered macrophage or neutrophil populations compared to saline-treated mice (Fig. 7A and B). However, the percentage of myeloid dendritic cells in the liver was significantly increased in the N:P 15 group (no PA), relative to mice treated with PBS and to all of the siPA-NPs (Fig. 7C). The average percentage of non-myeloid dendritic cells (DCs), which may include lymphoid and plasmacytoid DCs, for the N:P 15 group was also increased compared to saline and other NP formulations, though not significantly (Fig. 7D). Because the 15 group contained the highest N:P ratio for a non-PA-siRNA formulation, our data suggest that less stabilized si-NPs with higher ratios of polymer to siRNA stimulated a DC response in the liver. Liver DCs are known to be antigen-presenting and may be increased in number in response to inflammation or fibrosis [57]. Liver Kupffer cells, a primary phagocyte for intravenously delivered nanoparticles in general, are known to secrete IL-10, which can further recruit DCs to the liver [58]. Because the N:P 15 group also showed some elevations in IL-10 12 h after the final injection, this effect on DC levels may be due to activation of the Kupffer cells by N:P 15 si-NPs. Previous work has also shown that an i.v. injection of colloidal carbon resulted in increased recruitment of dendritic cells from circulation to the liver, indicating that this could be an underappreciated response to intravenous nanoparticle treatments [59]. Additionally, the presence of PA-siRNA in siPA-NP formulations appears to have a protective effect, since the 15 PA and 20 PA groups did not show signs of increased percentages of dendritic cells. While hepatic DCs can elicit a T cell response, we did not see any increase in liver T cells or B cells in any of the NP formulations (Supplemental Fig. 9A and B) [59,60]. Example gating for all lymphocyte populations can be found in Supplemental Fig. 10.

A common concern with long-term, repeated administration of PEGylated nanocarriers is the development of an immunogenic antibody response against PEG, which can diminish their efficacy as delivery vehicles and lead to clinical adverse events [61–63]. However, the immunogenicity of zwitterionic phosphocholine-nanocarriers has been less extensively measured, particularly after long-term injection courses [40]. We therefore tested the serum of mice injected six times over a month with our longest-circulating zwitterionic siPA-NPs (15 PA and 20 PA), for antibodies against phosphocholine using an ELISA-based assay [64,65]. There were no significant increases in ELISA signal for any of the mice sera sampled, indicating the complete absence of

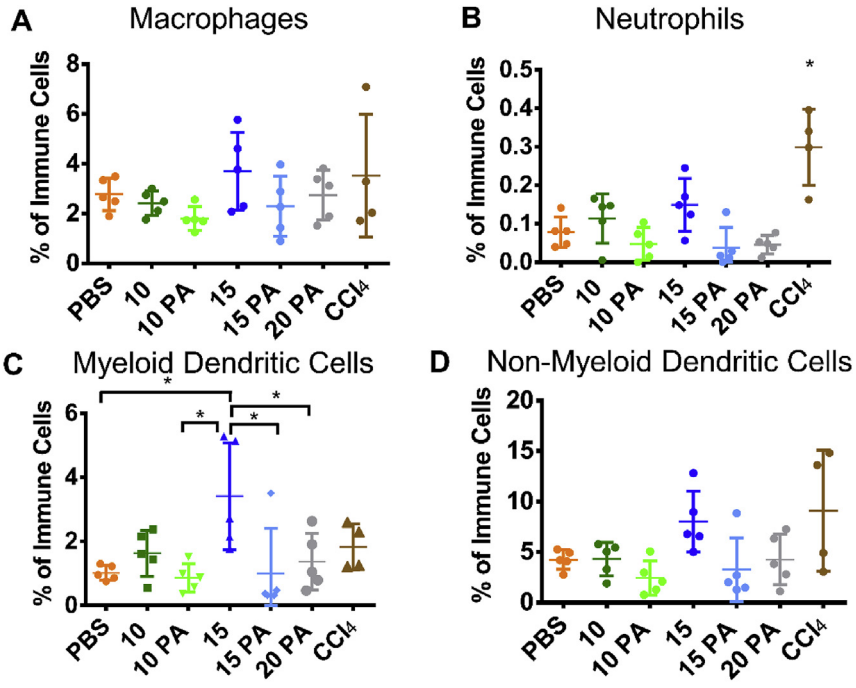

Fig. 7. Analysis of immune cell types in treated mouse livers. None of the NP formulations had significantly increased macrophages or neutrophils (A–B). However, si-NPs formulated at N:P 15 had (C) significantly increased myeloid dendritic cells compared to saline-treated mice and all other NP-treated mice except in the N:P 10 group ($n = 5$, $p < 0.05$). (D) Mice treated with si-NPs at N:P 15 also had elevated non-myeloid dendritic cells, though no groups had significantly increased non-myeloid dendritic cells compared to untreated controls.

anti-phosphocholine in these samples (Supplemental Fig. 11). Notably, positive control mouse sera containing phosphocholine antibodies did react with our polymers adsorbed to the plate, giving a positive ELISA signal. Thus, our long-circulating, dual hydrophobized siPA-NP formulations do not stimulate anti-PC immunogenicity in mice.

Taken together, our data show that zwitterated NPs are well-tolerated upon long-term, repeated administration, evidenced particularly by the normal body weight and complete blood count data. However, we have also demonstrated that the formulation N:P ratio and degree of hydrophobic core stabilization can significantly impact less pronounced markers of nanocarrier toxicology. The siPA-NPs at the highest overall polymer dose (20 PA) tested in the repeat injection studies exhibited mildly upregulated signs of hepatotoxicity based on liver enzymes, histology, and cytokines. Similarly, si-NPs at the highest polymer dose without palmitic acid-siRNA stabilization (15) also exhibited histological, cytokine, and liver dendritic cell responses. Our data indicate that a dual hydrophobization strategy can be used to improve the balance between improved pharmacokinetics and toxicologic factors, as the siPA-NP 15 PA formulation showed negligible signs of toxicity.

The polymer-induced toxicities that we observed are likely a result of destabilization and extracellular exposure of the cationic DMAEMA-containing polymer block. Although they are a driving force for siRNA delivery, cationic polymer components can be associated with aggregation of intracellular and extracellular proteins or unwanted membrane disruption [66–70]. While the positive charge density can be effectively shielded or reduced using hydrophilic NP corona-forming polymers and by copolymerization with other monomers, polyelectrolyte complexes are still prone to destabilization by serum and ionic blood or tissue components. Dual hydrophobization strategies improve NP stabilization and therefore may ameliorate toxicity concerns.

3.7. *In vivo luciferase knockdown and tumor biodistribution of lead siPA-NP formulations vs. Jet PEI*

Based on the favorable long-term toxicity data of the 15 PA siPA-NPs, and their identical pharmacokinetic area under the curves to the long-circulating, high N:P ratio NPs (20 and 20 PA), we compared this optimal formulation to the commercially available *in vivo*-jetPEI® (IVJP) in an orthotopic murine breast cancer model. At 24 h after intravenous administration, 15 PA siPA-NPs show significantly improved tumor luciferase silencing *in vivo* compared to IVJP formulations relative to matched scrambled controls (Fig. 8A and B). We also performed flow cytometry analysis on extracted tumors after administration of NPs bearing fluorescently-labeled nucleic acids, and we demonstrated a significant, 2.5-fold increased mean fluorescence intensity in tumors for 15 PA siPA-NPs compared to IVJP also at 24 h after injection (Fig. 8C), indicating better uptake and retention in tumor cells. Our NP optimization process, incorporating *in vivo* charge ratio screening and dual hydrophobization, therefore enables efficient tumor cell delivery and target gene knockdown *in vivo*, outperforming the only (to our knowledge) commercially available intravenously-injectable siRNA delivery reagent.

4. Conclusion

This work comprehensively characterizes the *in vivo* impacts of charge ratio and dual carrier-cargo hydrophobization on NP pharmacokinetics and toxicology. Increasing polymer given equal siRNA doses can significantly improve circulation half-life and area under the curve. These pharmacokinetic benefits may come at a cost of increased toxicity, particularly hepatic toxicities, but these can be overcome through dual hydrophobization—using hydrophobically modified siRNAs with partially hydrophobic polymeric NP cores. Our findings indicate that testing of electrostatically-complexed NPs at different charge ratios should extend to *in vivo* experiments, as the charge ratio may have a major impact on circulation kinetics, which is not evident *in vitro*. We've shown that dual hydrophobization significantly decreases toxicity while also increasing the circulation half-lives of NPs formulated at lower N:P ratios. Thus, dual hydrophobization allows for equivalent pharmacokinetic profiles at decreased polymer doses, reducing toxicity and increasing the potential for therapeutic efficacy.

This work also uniquely and deeply investigated the long-term impact of repeated administration of zwitterionic polyplexes, encompassing the impact of formulation parameters on their toxicology. We show that overall, zwitterionic polyplexes are well-tolerated upon repeated administration, with minimal histologic or immunologic consequences. Furthermore, optimized zwitterionic siPA-NP formulations are non-immunogenic and achieve improved tumor gene knockdown and biodistribution compared to commercial gold standards *in vivo*. Our work demonstrates that charge ratio optimization is important *in vivo* and that dual hydrophobization strategies improve delivery while overcoming the toxicologic challenges that face all electrostatically-

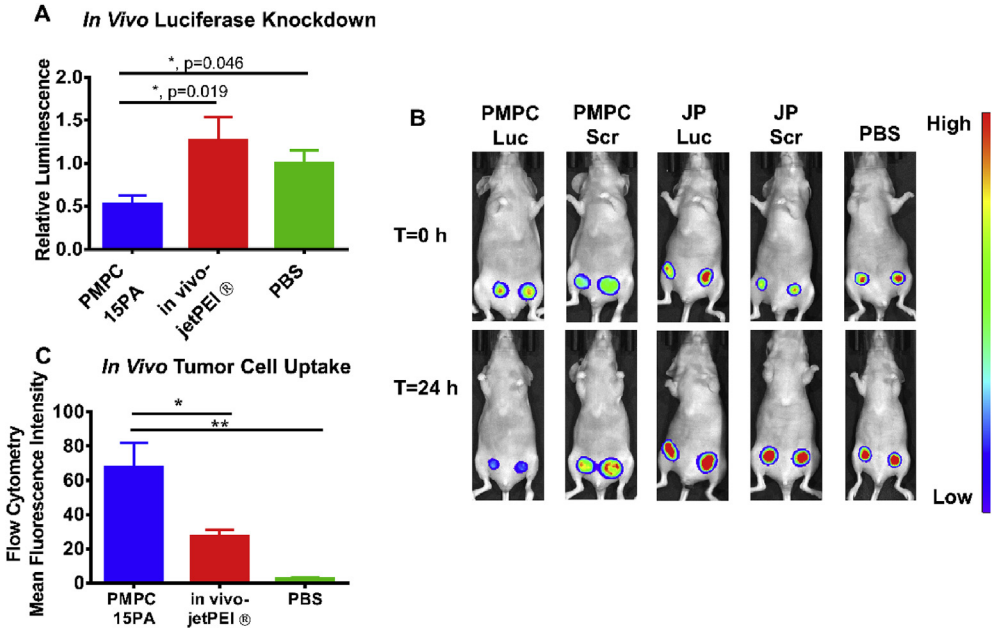

Fig. 8. NPs formulated at 15 PA (PMPC) display significantly increased knockdown (*p < 0.02) (A,B) and tumor uptake (C) *in vivo* compared to equivalent doses of In Vivo Jet-PEI® (JP) in nude mice bearing MDA-MB-231 tumors (*p < 0.02, **p < 0.01). (A) 1 mg/kg siPA-NPs bearing luciferase siRNA were injected in mice bearing 100 mm^3 tumors, and luminescent signals were monitored immediately before and 24 h after injection. Luminescence at t = 24 h relative to t = 0 h was compared relative to appropriate scrambled control groups. (B) Representative images of tumor luminescence from each treatment group bearing either luciferase (Luc) or scrambled (Scr) siRNA. (C) siPA-NPs bearing Cy5-labeled nucleic acids were injected intravenously in tumor-bearing mice. Tumors were collected 24 h after intravenous injection and analyzed for uptake by flow cytometry.

complexed polymeric siRNA carriers.

Data availability

The raw/processed data required to reproduce these findings are available upon request.

Acknowledgements

The authors acknowledge the assistance of the Vanderbilt Hormone and Analytical Services Core (NIH DK059637 and NIH DK020593) for plasma cytokine measurements.

The authors additionally acknowledge the assistance of the Vanderbilt Translational Pathology Shared Resource (TPSR) for serum chemistry and complete blood counts. TPSR is supported by NCI/NIH Cancer Center Support Grant 2P30 CA068485-14 and the Vanderbilt Mouse Metabolic Phenotyping Center Grant 5U24DK059637-13.

Flow cytometry experiments were performed in the Vanderbilt Medical Center Flow Cytometry Shared Resource (supported by the Vanderbilt Ingram Cancer Center [P30 CA68485] and the Vanderbilt Digestive Disease Research Center [DK058404]).

We are grateful to the DOD (DOD CDMRP OR130302), NIH (NIH R01 CA224241, NIH R01 EB019409, NIH R01 DK084246), NSF CAREER BMAT 1349604, the Vanderbilt Engineering and Immunity Pilot and Feasibility Grant, and the National Science Foundation (NSF GRF 1445197) for support.

The authors confirm that there are no known conflicts of interest associated with this publication and there has been no significant financial support for this work that could have influenced its outcome.

Appendix A. Supplementary data

Supplementary data to this article can be found online at https://doi.org/10.1016/j.biomaterials.2018.11.010.

References

[1] D. Adams, A. Gonzalez-Duarte, W. O'Riordan, C.-C. Yang, T. Yamashita, A. Kristen, I. Tournev, H. Schmidt, T. Coelho, J.L. Berk, K.-P. Lin, P.J. Dyck, P. Gandhi, M. Sweetser, J. Chen, S. Goyal, J. Gollob, O. Suhr, Patisiran, an investigational RNAi therapeutic for patients with hereditary transthyretin-mediated (hATTR) amyloidosis with polyneuropathy: results from the phase 3 APOLLO study (CT.001), Neurology 90 (15 Supplement) (2018).

[2] J. Wang, Z. Lu, M.G. Wientjes, J.L. Au, Delivery of siRNA therapeutics: barriers and carriers, AAPS J. 12 (4) (2010) 492–503.

[3] D. Haussecker, Current issues of RNAi therapeutics delivery and development, J. Contr. Release 195 (2014) 49–54.

[4] J.C. Kaczmarek, P.S. Kowalski, D.G. Anderson, Advances in the delivery of RNA therapeutics: from concept to clinical reality, Genome Med. 9 (2017) 60.

[5] T.A. Werfel, S. Wang, M.A. Jackson, T.E. Kavanaugh, M. Morrison Joly, L. Lee, D.J. Hicks, V. Sanchez, P.I. Gonzalez-Ericsson, K.V. Kilchrist, S.C. Dimobi, S.M. Sarett, D.M. Brantley-Sieders, R.S. Cook, C. Duvall, Selective MTORC2 Inhibitor Therapeutically Blocks Breast Cancer Cell Growth and Survival, Cancer Research, 2018.

[6] H. Li, C.E. Nelson, B.C. Evans, C.L. Duvall, Delivery of intracellular-acting biologics in pro-apoptotic therapies, Curr. Pharmaceut. Des. 17 (3) (2011) 293–319.

[7] C.V. Dang, E.P. Reddy, K.M. Shokat, L. Soucek, Drugging the 'undruggable' cancer targets, Nat. Rev. Canc. 17 (2017) 502.

[8] A. Wittrup, J. Lieberman, Knocking down disease: a progress report on siRNA therapeutics, Nat. Rev. Genet. 16 (9) (2015) 543–552.

[9] D. Papahadjopoulos, T.M. Allen, A. Gabizon, E. Mayhew, K. Matthay, S.K. Huang, K.D. Lee, M.C. Woodle, D.D. Lasic, C. Redemann, Sterically stabilized liposomes: improvements in pharmacokinetics and antitumor therapeutic efficacy, Proc. Natl. Acad. Sci. U. S. A. 88 (24) (1991) 11460–11464.

[10] J.W. Nichols, Y.H. Bae, Odyssey of a cancer nanoparticle: from injection site to site of action, Nano Today 7 (6) (2012) 606–618.

[11] M.A. Jackson, T.A. Werfel, E.J. Curvino, F. Yu, T.E. Kavanaugh, S.M. Sarett, M.D. Dockery, K.V. Kilchrist, A.N. Jackson, T.D. Giorgio, C.L. Duvall, Zwitterionic nanocarrier surface chemistry improves siRNA tumor delivery and silencing activity relative to polyethylene glycol, ACS Nano 11 (6) (2017) 5680–5696.

[12] T.A. Werfel, M.A. Jackson, T.E. Kavanaugh, K.C. Kirkbride, M. Miteva, T.D. Giorgio, C. Duvall, Combinatorial optimization of PEG architecture and hydrophobic content improves ternary siRNA polyplex stability, pharmacokinetics, and potency in vivo, J. Contr. Release 255 (2017) 12–26.

[13] S.M. Sarett, T.A. Werfel, I. Chandra, M.A. Jackson, T.E. Kavanaugh, M.E. Hattaway, T.D. Giorgio, C.L. Duvall, Hydrophobic interactions between polymeric Carrier and palmitic acid-conjugated siRNA improve PEGylated polyplex stability and enhance in vivo pharmacokinetics and tumor gene silencing, Biomaterials 97 (2016) 122–132.

[14] S.M. Sarett, T.A. Werfel, L. Lee, M.A. Jackson, K.V. Kilchrist, D. Brantley-Sieders, C.L. Duvall, Lipophilic siRNA targets albumin in situ and promotes bioavailability, tumor penetration, and Carrier-free gene silencing, Proceedings of the National Academy of Sciences, 2017.

[15] A. Gabizon, D. Papahadjopoulos, Liposome formulations with prolonged circulation time in blood and enhanced uptake by tumors, Proc. Natl. Acad. Sci. Unit. States Am. 85 (18) (1988) 6949.

[16] A. Gabizon, R. Catane, B. Uziely, B. Kaufman, T. Safra, R. Cohen, F. Martin, A. Huang, Y. Barenholz, Prolonged circulation time and enhanced accumulation in malignant exudates of doxorubicin encapsulated in polyethylene-glycol coated liposomes, Cancer Res. 54 (4) (1994) 987.

[17] E. Blanco, H. Shen, M. Ferrari, Principles of nanoparticle design for overcoming biological barriers to drug delivery, Nat. Biotechnol. 33 (2015) 941.

[18] J.E. Zuckerman, C.H. Choi, H. Han, M.E. Davis, Polycation-siRNA nanoparticles can disassemble at the kidney glomerular basement membrane, Proc. Natl. Acad. Sci. U. S. A. 109 (8) (2012) 3137–3142.

[19] B. Naeye, H. Deschout, V. Caveliers, B. Descamps, K. Braeckmans, C. Vanhove, J. Demeester, T. Lahoutte, S.C. De Smedt, K. Raemdonck, In vivo disassembly of IV administered siRNA matrix nanoparticles at the renal filtration barrier, Biomaterials 34 (9) (2013) 2350–2358.

[20] F. Alexis, E. Pridgen, L.K. Molnar, O.C. Farokhzad, Factors affecting the clearance and biodistribution of polymeric nanoparticles, Mol. Pharm. 5 (4) (2008) 505–515.

[21] S. Agarwal, Y. Zhang, S. Maji, A. Greiner, PDMAEMA based gene delivery materials, Mater. Today 15 (9) (2012) 388–393.

[22] A. Sato, S.W. Choi, M. Hirai, A. Yamayoshi, R. Moriyama, T. Yamano, M. Takagi, A. Kano, A. Shimamoto, A. Maruyama, Polymer brush-stabilized polyplex for a siRNA Carrier with long circulatory half-life, J. Contr. Release 122 (3) (2007) 209–216.

[23] O.M. Merkel, D. Librizzi, A. Pfestroff, T. Schurrat, K. Buyens, N.N. Sanders, S.C. De Smedt, M. Béhé, T. Kissel, Stability of siRNA polyplexes from poly(ethylenimine) and poly(ethylenimine)-g-poly(ethylene glycol) under in vivo conditions: effects on pharmacokinetics and biodistribution measured by Fluorescence Fluctuation Spectroscopy and Single Photon Emission Computed Tomography (SPECT) imaging, J. Contr. Release 138 (2) (2009) 148–159.

[24] J.E. Zuckerman, I. Gritli, A. Tolcher, J.D. Heidel, D. Lim, R. Morgan, B. Chmielowski, A. Ribas, M.E. Davis, Y. Yen, Correlating animal and human phase Ia/Ib clinical data with CALAA-01, a targeted, polymer-based nanoparticle containing siRNA, Proc. Natl. Acad. Sci. Unit. States Am. 111 (31) (2014) 11449–11454.

[25] H. Lv, S. Zhang, B. Wang, S. Cui, J. Yan, Toxicity of cationic lipids and cationic polymers in gene delivery, J. Contr. Release 114 (1) (2006) 100–109.

[26] S. Naahidi, M. Jafari, F. Edalat, K. Raymond, A. Khademhosseini, P. Chen, Biocompatibility of engineered nanoparticles for drug delivery, J. Contr. Release 166 (2) (2013) 182–194.

[27] M. Breunig, U. Lungwitz, R. Liebl, A. Goepferich, Breaking up the correlation between efficacy and toxicity for nonviral gene delivery, Proc. Natl. Acad. Sci. U. S. A. 104 (36) (2007) 14454–14459.

[28] H.J. Kim, A. Kim, K. Miyata, K. Kataoka, Recent progress in development of siRNA delivery vehicles for cancer therapy, Adv. Drug Deliv. Rev. 104 (2016) 61–77.

[29] J.J. Green, R. Langer, D.G. Anderson, A combinatorial polymer library approach yields insight into nonviral gene delivery, Acc. Chem. Res. 41 (6) (2008) 749–759.

[30] D.J. Siegwart, K.A. Whitehead, L. Nuhn, G. Sahay, H. Cheng, S. Jiang, M. Ma, A. Lytton-Jean, A. Vegas, P. Fenton, C.G. Levins, K.T. Love, H. Lee, C. Cortez, S.P. Collins, Y.F. Li, J. Jang, W. Querbes, C. Zurenko, T. Novobrantseva, R. Langer, D.G. Anderson, Combinatorial synthesis of chemically diverse core-shell nanoparticles for intracellular delivery, Proc. Natl. Acad. Sci. Unit. States Am. 108 (32) (2011) 12996.

[31] H. Cabral, K. Miyata, K. Osada, K. Kataoka, Block copolymer micelles in nanomedicine applications, Chem. Rev. 118 (14) (2018) 6844–6892.

[32] R.E.B. Fitzsimmons, H. Uludağ, Specific effects of PEGylation on gene delivery efficacy of polyethylenimine: interplay between PEG substitution and N/P ratio, Acta Biomater. 8 (11) (2012) 3941–3955.

[33] A. Malek, O. Merkel, L. Fink, F. Czubayko, T. Kissel, A. Aigner, In vivo pharmacokinetics, tissue distribution and underlying mechanisms of various PEI(–PEG)/siRNA complexes, Toxicol. Appl. Pharmacol. 236 (1) (2009) 97–108.

[34] F. Verbaan, I. van Dam, Y. Takakura, M. Hashida, W. Hennink, G. Storm, C. Oussoren, Intravenous fate of poly(2-(dimethylamino)ethyl methacrylate)-based polyplexes, Eur. J. Pharmaceut. Sci. 20 (4) (2003) 419–427.

[35] S. Kawakami, Y. Ito, P. Charoensit, F. Yamashita, M. Hashida, Evaluation of proinflammatory cytokine production induced by linear and branched polyethylenimine/plasmid DNA complexes in mice, J. Pharmacol. Exp. Therapeut. 317 (3) (2006) 1382.

[36] Y. Yue, F. Jin, R. Deng, J. Cai, Y. Chen, M.C.M. Lin, H.-F. Kung, C. Wu, Revisit complexation between DNA and polyethylenimine — effect of uncomplexed chains free in the solution mixture on gene transfection, J. Contr. Release 155 (1) (2011) 67–76.

[37] M. Thibault, M. Astolfi, N. Tran-Khanh, M. Lavertu, V. Darras, A. Merzouki, M.D. Buschmann, Excess polycation mediates efficient chitosan-based gene transfer by promoting lysosomal release of the polyplexes, Biomaterials 32 (20) (2011) 4639–4646.

[38] F.J. Verbaan, P.K. Klouwenberg, J.H.v. Steenis, C.J. Snel, O. Boerman,

W.E. Hennink, G. Storm, Application of poly(2-(dimethylamino)ethyl methacrylate)-based polyplexes for gene transfer into human ovarian carcinoma cells, Int. J. Pharm. 304 (1) (2005) 185–192.
[39] C.E. Nelson, J.R. Kintzing, A. Hanna, J.M. Shannon, M.K. Gupta, C.L. Duvall, Balancing cationic and hydrophobic content of PEGylated siRNA polyplexes enhances endosome escape, stability, blood circulation time, and bioactivity in vivo, ACS Nano 7 (10) (2013) 8870–8880.
[40] P. Zhang, F. Sun, C. Tsao, S. Liu, P. Jain, A. Sinclair, H.C. Hung, T. Bai, K. Wu, S. Jiang, Zwitterionic gel encapsulation promotes protein stability, enhances pharmacokinetics, and reduces immunogenicity, Proc. Natl. Acad. Sci. U. S. A. 112 (39) (2015) 12046–12051.
[41] Y. Men, S. Peng, P. Yang, Q. Jiang, Y. Zhang, B. Shen, P. Dong, Z. Pang, W. Yang, Biodegradable zwitterionic nanogels with long circulation for antitumor drug delivery, ACS Appl. Mater. Interfaces 10 (28) (2018) 23509–23521.
[42] H.J. Kim, A. Ishii, K. Miyata, Y. Lee, S. Wu, M. Oba, N. Nishiyama, K. Kataoka, Introduction of stearoyl moieties into a biocompatible cationic polyaspartamide derivative, PAsp(DET), with endosomal escaping function for enhanced siRNA-mediated gene knockdown, J. Contr. Release 145 (2) (2010) 141–148.
[43] H.J. Kim, K. Miyata, T. Nomoto, M. Zheng, A. Kim, X. Liu, H. Cabral, R.J. Christie, N. Nishiyama, K. Kataoka, siRNA delivery from triblock copolymer micelles with spatially-ordered compartments of PEG shell, siRNA-loaded intermediate layer, and hydrophobic core, Biomaterials 35 (15) (2014) 4548–4556.
[44] Y. Oe, R.J. Christie, M. Naito, S.A. Low, S. Fukushima, K. Toh, Y. Miura, Y. Matsumoto, N. Nishiyama, K. Miyata, K. Kataoka, Actively-targeted polyion complex micelles stabilized by cholesterol and disulfide cross-linking for systemic delivery of siRNA to solid tumors, Biomaterials 35 (27) (2014) 7887–7895.
[45] K. Nishina, T. Unno, Y. Uno, T. Kubodera, T. Kanouchi, H. Mizusawa, T. Yokota, Efficient in vivo delivery of siRNA to the liver by conjugation of α-tocopherol, Mol. Ther. 16 (4) (2008) 734–740.
[46] T. Kubo, Y. Takei, K. Mihara, K. Yanagihara, T. Seyama, Amino-modified and lipid-conjugated dicer-substrate siRNA enhances RNAi efficacy, Bioconjug. Chem. 23 (2) (2012) 164–173.
[47] V.V. Ambardekar, H.Y. Han, M.L. Varney, S.V. Vinogradov, R.K. Singh, J.A. Vetro, The modification of siRNA with 3' cholesterol to increase nuclease protection and suppression of native mRNA by select siRNA polyplexes, Biomaterials 32 (5) (2011) 1404–1411.
[48] B.C. Evans, C.E. Nelson, S.S. Yu, K.R. Beavers, A.J. Kim, H. Li, H.M. Nelson, T.D. Giorgio, C.L. Duvall, Ex vivo red blood cell hemolysis assay for the evaluation of pH-responsive endosomolytic agents for cytosolic delivery of biomacromolecular drugs, JoVE : JoVE 73 (2013) 50166.
[49] J.L. Betker, T.J. Anchordoquy, Effect of charge ratio on lipoplex-mediated gene delivery and liver toxicity, Ther. Deliv. 6 (11) (2015) 1243–1253.
[50] H. Maeda, H. Nakamura, J. Fang, The EPR effect for macromolecular drug delivery to solid tumors: improvement of tumor uptake, lowering of systemic toxicity, and distinct tumor imaging in vivo, Adv. Drug Deliv. Rev. 65 (1) (2013) 71–79.
[51] V. Torchilin, Tumor delivery of macromolecular drugs based on the EPR effect, Adv. Drug Deliv. Rev. 63 (3) (2011) 131–135.
[52] A.J. Clark, D.T. Wiley, J.E. Zuckerman, P. Webster, J. Chao, J. Lin, Y. Yen, M.E. Davis, CRLX101 nanoparticles localize in human tumors and not in adjacent, nonneoplastic tissue after intravenous dosing, Proc. Natl. Acad. Sci. U. S. A. 113 (14) (2016) 3850–3854.
[53] M. Zheng, D. Librizzi, A. Kılıç, Y. Liu, H. Renz, O.M. Merkel, T. Kissel, Enhancing in vivo circulation and siRNA delivery with biodegradable polyethylenimine-graft-polycaprolactone-block-poly(ethylene glycol) copolymers, Biomaterials 33 (27) (2012) 6551–6558.
[54] R.J. Christie, K. Miyata, Y. Matsumoto, T. Nomoto, D. Menasco, T.C. Lai, M. Pennisi, K. Osada, S. Fukushima, N. Nishiyama, Y. Yamasaki, K. Kataoka, Effect of polymer structure on micelles formed between siRNA and cationic block copolymer comprising thiols and amidines, Biomacromolecules 12 (9) (2011) 3174–3185.
[55] R.J. Christie, Y. Matsumoto, K. Miyata, T. Nomoto, S. Fukushima, K. Osada, J. Halnaut, F. Pittella, H.J. Kim, N. Nishiyama, K. Kataoka, Targeted polymeric micelles for siRNA treatment of experimental cancer by intravenous injection, ACS Nano 6 (6) (2012) 5174–5189.
[56] J.E. Zuckerman, M.E. Davis, Clinical experiences with systemically administered siRNA-based therapeutics in cancer, Nat. Rev. Drug Discov. 14 (12) (2015) 843–856.
[57] A.H. Rahman, C. Aloman, Dendritic cells and liver fibrosis, Biochim. Biophys. Acta (BBA) - Mol. Basis Dis. 1832 (7) (2013) 998–1004.
[58] F. Heymann, F. Tacke, Immunology in the liver — from homeostasis to disease, Nat. Rev. Gastroenterol. Hepatol. 13 (2016) 88.
[59] A.H. Lau, A.W. Thomson, Dendritic cells and immune regulation in the liver, Gut 52 (2) (2003) 307–314.
[60] M.W. Robinson, C. Harmon, C. O'Farrelly, Liver immunology and its role in inflammation and homeostasis, Cell. Mol. Immunol. 13 (2016) 267.
[61] P. Zhang, F. Sun, S. Liu, S. Jiang, Anti-PEG antibodies in the clinic: current issues and beyond PEGylation, J. Contr. Release 244 (Pt B) (2016) 184–193.
[62] Y.-C. Hsieh, H.-E. Wang, W.-W. Lin, S.R. Roffler, T.-C. Cheng, Y.-C. Su, J.-J. Li, C.-C. Chen, C.-H. Huang, B.-M. Chen, J.-Y. Wang, T.-L. Cheng, F.-M. Chen, Pre-existing anti-polyethylene glycol antibody reduces the therapeutic efficacy and pharmacokinetics of PEGylated liposomes, Theranostics 8 (11) (2018) 3164–3175.
[63] Y. Qi, A. Simakova, N.J. Ganson, X. Li, K.M. Luginbuhl, I. Ozer, W. Liu, M.S. Hershfield, K. Matyjaszewski, A. Chilkoti, A brush-polymer/exendin-4 conjugate reduces blood glucose levels for up to five days and eliminates poly(ethylene glycol) antigenicity, Nat. Biomed. Eng. 1 (2016) 0002.
[64] T. Ishihara, M. Takeda, H. Sakamoto, A. Kimoto, C. Kobayashi, N. Takasaki, K. Yuki, K. Tanaka, M. Takenaga, R. Igarashi, T. Maeda, N. Yamakawa, Y. Okamoto, M. Otsuka, T. Ishida, H. Kiwada, Y. Mizushima, T. Mizushima, Accelerated blood clearance phenomenon upon repeated injection of PEG-modified PLA-nanoparticles, Pharm. Res. 26 (10) (2009) 2270–2279.
[65] T. Ishihara, T. Maeda, H. Sakamoto, N. Takasaki, M. Shigyo, T. Ishida, H. Kiwada, Y. Mizushima, T. Mizushima, Evasion of the accelerated blood clearance phenomenon by coating of nanoparticles with various hydrophilic polymers, Biomacromolecules 11 (10) (2010) 2700–2706.
[66] P.R. Leroueil, S. Hong, A. Mecke, J.R. Baker, B.G. Orr, M.M. Banaszak Holl, Nanoparticle interaction with biological membranes: does nanotechnology present a janus face? Acc. Chem. Res. 40 (5) (2007) 335–342.
[67] J. Chen, J.A. Hessler, K. Putchakayala, B.K. Panama, D.P. Khan, S. Hong, D.G. Mullen, S.C. DiMaggio, A. Som, G.N. Tew, A.N. Lopatin, J.R. Baker, M.M.B. Holl, B.G. Orr, Cationic nanoparticles induce nanoscale disruption in living cell plasma membranes, J. Phys. Chem. B 113 (32) (2009) 11179–11185.
[68] S.M. Moghimi, P. Symonds, J.C. Murray, A.C. Hunter, G. Debska, A. Szewczyk, A two-stage poly(ethylenimine)-mediated cytotoxicity: implications for gene transfer/therapy, Mol. Ther. 11 (6) (2005) 990–995.
[69] G. Grandinetti, A.E. Smith, T.M. Reineke, Membrane and nuclear permeabilization by polymeric pDNA vehicles: efficient method for gene delivery or mechanism of cytotoxicity? Mol. Pharm. 9 (3) (2012) 523–538.
[70] B. Ballarín-González, K.A. Howard, Polycation-based nanoparticle delivery of RNAi therapeutics: adverse effects and solutions, Adv. Drug Deliv. Rev. 64 (15) (2012) 1717–1729.